

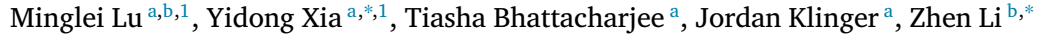
Contents lists available at ScienceDirect

Powder Technology

journal homepage: www.journals.elsevier.com/powder-technology



Predicting biomass comminution: Physical experiment, population balance model, and deep learning

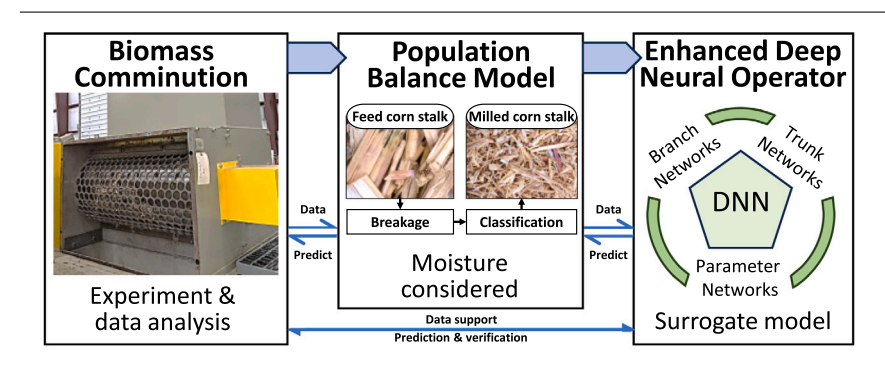


- ^a Energy and Environment Science & Technology, Idaho National Laboratory, Idaho Fall, ID 83415, USA
- ^b Department of Mechanical Engineering, Clemson University, Clemson, SC 29634, USA

HIGHLIGHTS

- An extended population balance model (PBM) is developed for biomass comminution.
- Biomass feed moisture is added in the PBM as a new input parameter.
- An enhanced deep neutral operator (DNO+) model is developed for biomass comminution.
- DNO+ allows for influencing factors such as moisture and screen size as extra inputs
- Both models are remarkably accurate in the calibration or training parameter space.

GRAPHICAL ABSTRACT



ARTICLE INFO

Keywords:
Corn stover
Preprocessing
Knife mill
Machine learning
Deep neural operator

ABSTRACT

An extended population balance model (PBM) and a deep learning-based enhanced deep neural operator (DNO+) model are introduced for predicting particle size distribution (PSD) of comminuted biomass through a large knife mill. Experimental tests using corn stalks with varied moisture contents, mill blade speeds, and discharge screen sizes are conducted to support model development. A novel mechanism in the extended PBM allows for including additional input parameters such as moisture content, which is not possible in the original PBM. The DNO+ model can include influencing factors of different data types such as moisture content and discharge screen size, which significantly extends the engineering applicability of the standard DNO model that only admits feed PSD and outcome PSD. Test results show that both models are remarkably accurate in the calibration or training parameter space and can be used as surrogate models to provide effective guidance for biomass preprocessing design.

1. Introduction

Despite the growing production of biofuels and biochemicals, processes involving granular biomass remain not well understood or controlled in contrast to the processing of fluids [1]. Biomass preprocessing refers to unit operations in a biorefinery to improve bulk flowability, reduce cellulose crystallinity, increase biomass porosity, and enhance

enzyme accessibility [2]. As a critical step in biomass preprocessing, comminution plays a vital role in source material sorting and size reduction that increases the surface area and enhances the accessibility of biomass to the subsequent processes. Particle size distribution (PSD) of comminuted biomass is a critical material attribute that directly impacts materials handling and conversion performance [3]. However,

E-mail addresses: yidong.xia@inl.gov (Y. Xia), zli7@clemson.edu (Z. Li).

^{*} Corresponding authors.

¹ These authors contributed equally to this work.

Powder Technology 441 (2024) 119830

Nomenclature	
Symbols	
α	Fitting parameter related to breakage function characterization in the PBM
S	Vector for breakage probability
\mathbf{p}_{in}	Vector for mass percentage distribution of feed particles
$\mathbf{p}_{\mathrm{out}}$	Vector for mass percentage distribution of discharged particles
X	Vector for particle size sequence
В	Breakage function matrix
$oldsymbol{\Phi}_{ ext{in}}$	Vector for cumulative mass percentage distribution of feed particles
$oldsymbol{\Phi}_{ ext{out}}$	Vector for cumulative mass percentage distribution of discharged particles
\boldsymbol{C}	Classification matrix
g, f	Continuous vector functions
X	Breakage matrix
γ	Fitting parameter related to breakage function characterization in the PBM
${\mathcal F}$	Fully connected neural network operator
${\mathscr L}$	Convolutional neural network operator
μ	Mean value
ϕ	Activation function of neural network
σ	Standard deviation
CI	Confidence interval of measurement
d_{scr}	Screen size (m) Material's resistance to breaking under the
$f_{ m res}$	Material's resistance to breaking under the impact energy (kg J^{-1} m ⁻¹)
G, F, H	Nonlinear continuous operators
k	A superscript to denote the sequence of impact between mill knife and particles
M.C.	Moisture content (%)
$m_{ m dry}$	Mass of dried corn stalks (kg)
$m_{ m wet}$	Mass of water-treated corn stalks (kg)
q	Exponent of the heuristic power law
v	Linear velocity of the mill blade tip (m s ⁻¹)
$w_{ m kin}$	Impact specific kinetic energy (J kg ⁻¹)
$w_{ m min}$	Minimum specific energy required for
	breakage (J kg ⁻¹)
x_{\min}	Minimum particle size (m)
$\mathbf{m}^{(k)}$	Vector for mass percentage of impacted
$\mathbf{r}^{(k)}$	particles in mill chamber after <i>k</i> th impact Vector for mass percentage of remainder particles in mill chamber after <i>k</i> th impact
D10	Particle sieve size corresponding to 10% of
D50	cumulative mass (m)
D50	Particle sieve size corresponding to 50% of cumulative mass (m)
D90	Particle sieve size corresponding to 90% of
	cumulative mass (m)
DEM	Discrete Element Method
DNN	Deep Neural Network
DNO+	Enhanced Deep Neural Operator
DNO	Deep Neural Operator
PBM	Population Balance Model

almost no mill on the market is designed specifically for biomass comminution. In biomass preprocessing, how to properly operate an existing mill originally designed for other materials such as agricultural produces is less explored. The lack of knowledge to predict particle size distribution of comminuted biomass based on existing mills can result in the use of unsuitable material properties or mill processing parameters that contribute to process upsets such as material jamming or clogging in the transport and feeding operations, and eventually poor conversion and yield rate [4]. Predictive models for particle size distribution of comminuted biomass based on the feed material properties and mill processing parameters are desired for the optimal design of biomass preprocessing in a biorefinery. Computational models and analytical models have been developed and used for the comminution process in the past. A brief literature survey is as follows.

Computational models based on the discrete element method (DEM) have been used for simulating the comminution process by explicitly considering the inter-particle and particle-boundary interactions, and fragmentation phenomena [5]. Particle size distribution of comminuted materials depends on the complex interplay between feed material properties and mill processing parameters, encompassing coupled multi-physics mechanisms such as contact and fracture mechanics. surface physics, fluid dynamics, and even thermal effects on materials [6]. DEM simulations of attrition mills and crushing mills have been used to understand the comminution outcome as a function of material properties and mill processing parameters for hard-brittle materials, such as mineral ores [7], gravel [8], coal [9], pharmaceutical powders [10], lactose [11], and bone material [12]. More examples were summarized in a review on the contribution of DEM to the science of comminution [13]. In those DEM simulations, the fragmentation of brittle materials were modeled using a composite-particle approach [14,15], where larger primary particles were fabricated by "gluing" smaller particles with cohesive bonds. In this DEM model, particle breakage is not due to fracture or crack propagation, but due to bigger particles (agglomerates) disintegrating into clusters of smaller particles [16] based on predefined breakage functions [17]. In contrast to the hard-brittle materials aforementioned, biomass such as corn stover is much softer and flexible and thus, the DEM models that do not resolve particle deformation are not suitable for biomass. The recent introduction of various deformable DEM particle models [18], such as the bonded-sphere model [19] and bonded sphero-cylinder model [20], has made it possible to simulate the granular flow dynamics and breakage of biomass such as corn stalks [21,22], wheat stems [23,24], pinewood [25,26], and switchgrass [27]. Despite the value of DEM simulations to elucidate the criticality and optimal ranges of feed material properties and mill processing parameters, DEM simulations are too expensive for use to support the rapid design of biomass preprocessing pathways with changing feed materials and operating conditions. For example, it can take a few days to complete a DEM simulation of knife mill of one corn stalk on a workstation, depending on the stalk size and discharge screen size [28]. Therefore, predictive models of biomass comminution that do not require excessive computing time are desired by system engineers among industry stakeholders.

Analytical models based on the population balance model (PBM) for predicting comminution outcome have a firm theoretical foundation in probabilistic breakage mechanics based on the mean particle properties [29,30]. The development of PBM models [31,32] and their calibration against physical experimental data have focused on the comminution of hard-brittle materials such as acryl and limestone [33], and pharmaceutical extrudates [34]. In their pioneer work, Gil et al. [35] adapted the underlying theory of PBM to describe the breakage behavior of herbaceous biomass (corn stover) and woody biomass (poplar), respectively, under single impact in a laboratory bench-scale impact mill. Subsequently, Gil et al. [36] formally introduced PBM, as well as the classification system modeling and the calculation of the number of impact, and tested the model for the milling of different types of biomass in a laboratory bench-scale impact mill. Like the

calibration of DEM models, PBM models also require new experimental data for re-calibrating parameters when new materials are used in a tested mill, or for re-validation when a new mill is used for a tested material. Because PBM models do not track transient granular flow dynamics or fragmentation phenomena like DEM, they require literally negligible computing time in contrast to DEM, and therefore they are potential models for supporting the rapid design or re-configuration of biomass preprocessing pathways as part of a digital system. Despite the relative low cost of PBM, however, the current PBM theory has a limitation that it does not include moisture content (M.C.) as an input parameter, which is a critical material attribute influencing the comminution performance of not only biomass [37] but also other materials such as flowers [38] and food resources [39]. Furthermore, to the best of the authors' knowledge, the feasibility of PBM for biomass comminution at the bench scale [36] has not been investigated for application to production-scale mills.

In the meantime, the rapid advancement of machine learning (ML) technologies has attracted the attention of the bioenergy research community [40]. Machine learning enables accurate predictions based on the analysis of large volumes of complex data and the identification of sophisticated patterns, and can be considered as complementary approaches to PBM for predicting the performance of biomass feedstock preprocessing. Among the machine learning algorithms, deep neural network (DNN) models were designed to mimic the structure and functionality of human intelligence by enabling the process of learning from a vast amount of data. In the bioenergy research area, the deep neural network models showed promising results in applications such as classification of biomass constituents [41], biochar yield prediction [42,43], and optimization of biomass pyrolysis [44]. The further development of deep neural networks resulted in the deep neural operator (DNO) model that expands the capabilities of deep neural networks. DNO refers to a class of deep learning models specifically designed for solving complex mathematical and scientific problems [45-48]. Unlike the early neural network models designed to learn the mapping from inputs to outputs, DNO models learn the underlying operators or functions autonomously. These operators can be differential operators, integral operators, or other mathematical operators that are commonly encountered in scientific disciplines. So far, the machine learning method for predicting biomass comminution is relatively an unexplored area.

The objective of this work is to assess, improve, and extend the predictive models for biomass comminution beyond the bench-scale mill and toward the production-scale mill. The research effort consisted of three integral parts. First, corn stover and a production-scale knife mill were chosen for generating experimental testing data of biomass comminution to facilitate the development, calibration, and validation of new predictive models. Second, the feasibility of adapting the current PBM model for biomass comminution to the production-scale knife mill was assessed via calibration based on the experimental data. Also, a novel method was developed to incorporate the influence of feed moisture content in the PBM process. Third, a novel machine learningbased model, namely the enhanced deep neural operator (DNO+), was introduced for predicting the particle size distribution of comminuted biomass from the production-scale knife mill. The DNO+ model for biomass comminution incorporates the dynamic mapping function in the DNO algorithm [49], and in addition, takes into account of material properties and processing parameters that critically influence the outcome, such as feed moisture content and mill discharge screen size. This allows for the DNO+ model to overcome the limitation of the current PBM, and upon training, to acquire the ability to predict biomass comminution.

The remainder of this work is organized as follows. Section 2 introduces the experimental setup, equipment operation, and data acquisition in support of the model development. Section 3 describes the PBM and DNO+ models. Section 4 presents the results of the models for predicting particle size distribution of comminuted corn stover given different feed particle size distribution, discharge screen sizes, and feed moisture contents as model inputs. Finally, Section 5 concludes the main findings of this work.

2. Experimental methods

Manually sorted corn stalks were used as the research sample instead of whole corn stover that contains various anatomical fractions such stalks, husks, leaves, and cobs [50]. Each anatomical fraction has very different size ranges and material attributes, and thus can behave very differently in a comminution process. The effort to understand the comminution of all individual anatomical fractions is beyond the present scope. Since stalks account for the biggest mass fraction of corn stover (about 50%), the use of stalks is representative in this study and avoids influence from other anatomical fractions. An experimental comminution test was designed to investigate factors that can influence the particle size distribution of comminuted material. The objective of the test was to analyze the criticality of the factors (particle size distribution and moisture content of the feed material, blade tip speed, discharge screen size, etc.) on the comminution outcome, and provide experimental data to support the development of predictive models.

2.1. Milling equipment

A G1635 Granulator knife mill (Jordan Reduction Solutions (JRS), Birmingham, Alabama) [51] was used as the mechanical size reduction method for corn stalks in this study. A knife mill slices corn stalks and typically produces small pieces (similar to chopping with a knife) whereas a hammer mill grinds corn stalks and typically produces long thin pieces (similar to a mortar and pestle). More description about the mechanisms of different mills can be found in the literature [52]. The JRS knife mill is composed of several parts based on its structure: feed bin, mill throat, mill chamber, discharge screen, and collection bin, shown in Fig. 1. The mill throat consists of 2 stationary knives and 5 equally spaced rotary knives, each 0.895 m long, on a 0.362 m diameter rotor. The clearance between the stationary knives and rotary knives is about 0.3 mm. The tip speed of the rotary blade is about 10 m s^{-1} . The discharge screen has approximately 0.284 m² surface area, and changeable perforations from 76 mm (3 in.) to 6.35 mm (0.25 in.). The knife blades are made of hardened steel inlays and sharpened. A sharp knife edge ensures a consistent particle size distribution. If the knife edges are dull, they tend to crush or tear the material instead of delivering clean shear cut. In addition, excessive heat generated during milling can result in material degradation or even combustion, especially when processing biomass at low moisture content. To balance between the milling efficiency and the heat generated during the process, the knives are sharpened to a modest angle of 45 degrees.

2.2. Feeding approach

In this experimental test, corn stalks were fed into the feed bin individually with gap time between the feeding of each stalk to allow for sufficient milling and discharging. As a result, this excluded feeding mass rate as an influencing factor in the comminution outcome. Feeding mass rate was not considered as a variable parameter, because of the limited amount of manually sorted corn stalks needed for the parametric studies of parameters such as feed moisture content, blade tip speed, and discharge screen size. Therefore, the prediction models to be introduced in this work will not include time-dependent input parameters such as feeding mass rate, or output quantities such as discharging mass rate. It is worth noting that the DEM simulations resolve the transient motion and breakage of individual corn stalks in a knife mill and thus can predict the comminution time, though at the cost of tremendous computing time [28].

Before the comminution test, the dimensions of the corn stalks were measured manually with a digital caliper to the nearest 0.01 mm. If particle length, and breadth (major axis) and width (minor axis) of the approximate elliptic cross-sectional area are used to describe the particle dimensions of both the feed corn stalks and comminuted fragments, particle width is the smallest dimension and the particles

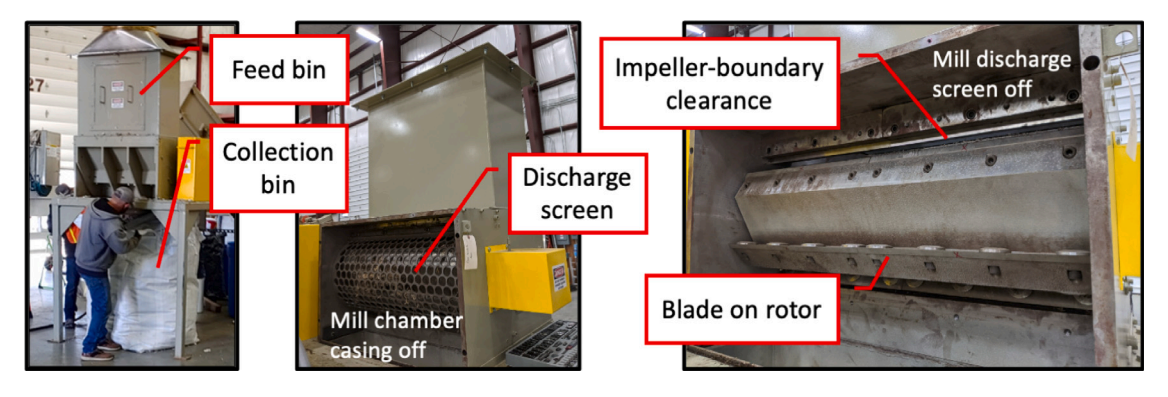


Fig. 1. Photograph of a G1635 Granulator knife mill system at Idaho National Laboratory.

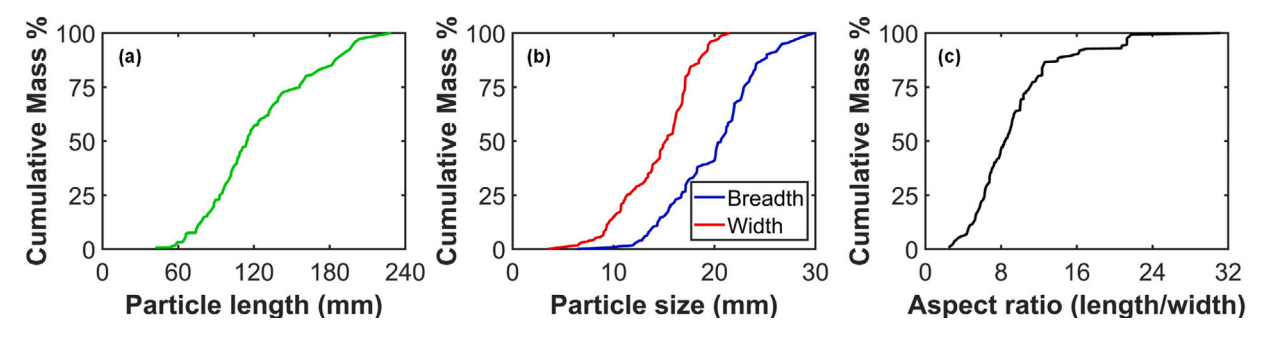


Fig. 2. Characterized dimensions of the initial corn stalk samples: (a) particle length distribution, (b) particle breadth and width distribution, and (c) aspect ratio distribution.

have a large aspect ratio of length and width [53]. The characterized dimensions of the feed corn stalks are shown in Fig. 2, which were based on an analytical split of over 300 measured corn stalks. To be consistent with the size characterization of the comminuted particles, the particle width distribution of the feed corn stalks is regarded as the particle size distribution of the feed material, shown as the red profile in Fig. 2b.

2.3. Moisture control

To prepare the comminution tests for the feed corn stalks at different levels of moisture content, water was added to the corn stalks gravimetrically to increase the moisture content. Notice that adding moisture can impact the properties of corn stalks. However, due to the logistics systems for the collection of corn stover after grain harvest, material bailing, storage, and feedstock queuing to supply a biorefinery for yearly operation with a crop that is harvested once a year, it is unrealistic that the properties and analysis should be based on the "green" stalk samples. The material used in this study were collected and baled from an operating farm in Iowa, and transported to Idaho National Laboratory. In the lab, the bale was opened and the stalks were recovered. From the time of harvest and baling through intermediate storage and then testing in the lab, the material naturally went through wetting/drying cycles due to climatic shifts, temperature changes, and precipitation events. For this study, all samples were treated the same from receipt at the lab and were never dried other than through natural conditions to limit hornification. From this point, it is adequate to add moisture to the stalk samples and allow them to equilibrate to represent similar real-case scenarios that a biorefinery might experience.

To determine the moisture content of the water-treated corn stalks, a small portion of the sample was collected from the batch and weighed to measure the mass $m_{\rm wet}$. The sample was then placed in a low-temperature oven for drying and then measured for its mass $m_{\rm dry}$. The dry corn stalks still contain about 5% moisture content as bonded water

in cells. The moisture content of water-treated corn stalks is measured by

$$M.C. = \frac{m_{\text{wet}} - m_{\text{dry}}}{m}.$$
 (1)

The samples used in the moisture measurement were discarded. The remaining material, assuming homogeneously water treated, underwent one of the two approaches to achieve the target moisture content for use in the comminution test. If the moisture content was higher than the target level, the material was then placed in a low-temperature oven for slow drying to reach the target moisture content. Conversely, more water was added to the material until the target moisture content was attained. Once the target moisture content was reached, the material was measured again to ensure that the actual moisture content was within a few percent of difference from the target value. It is crucial to store all the samples for at least 24 h before using them in the comminution test. Dry stalks were stored in sealed containers at room temperature. Water-treated stalks were stored in sealed containers in cold storage. These preparations ensured that the samples and water had sufficient time to equilibrate to reach a consistent moisture content in the samples.

2.4. Comminuted particle size measurement

A series of corn stalk comminution tests were conducted in the JRS knife mill with the different combinations of blade tip speed, feed moisture content, and discharge screen size, shown in Table 1. The screen size refers to the diameter of perforations on the discharge screen. In the mill chamber, corn stalks were size reduced to smaller particles upon impact with the blades. The particles that became sufficiently small to pass through the discharge screen fell into the collection bin. Almost all the materials eventually fell through and the mass percentage of the residual material inside the mill chamber was negligible.

Particle size distributions of comminuted particles were measured in a W.S. Tyler RX-30 Rotap (W.S. Tyler, Mentor, Ohio). This devices

Table 1
The list of physical testing conditions for the JRS knife mill operation of corn stalks.

Testing no.	Blade tip speed (m s ⁻¹)	Moisture content (%)	Screen size (mm)
1	6.5	20	12.70
2	6.5	20	19.05
3	6.5	40	12.70
4	6.5	40	19.05
5	8.2	20	12.70
6	8.2	20	19.05
7	8.2	40	12.70
8	8.2	40	19.05
9	9.8	20	12.70
10	9.8	20	19.05
11	9.8	40	12.70
12	9.8	40	19.05

uses a stack of selected analytical sieves, from largest to smallest, to separate particles using a rotational base and a tapping arm on top of the stack. For the comminuted particles collected from the 19.05 mm discharge screen, this study used 18 layers of sieves (i.e., 13.2, 11.2, 9.53, 6.35, 5.6, 3.35, 2.36, 2, 1.7, 1.4, 1.18, 1, 0.85, 0.71, 0.6, 0.425, 0.25, and 0.18 mm) along with a solid fines pan. or the comminuted particles collected from the 12.70 mm discharge screen, this study used 17 layers of sieves (i.e., 9.53, 6.35, 5.6, 3.35, 2.36, 2, 1.7, 1.4, 1.18, 1, 0.85, 0.71, 0.6, 0.425, 0.25, 0.18, and 0.15 mm) along with a solid fines pan. Sieve sizes represent approximately the smallest dimensions of comminuted corn stalks (i.e., particle width) and they correspond to the *particle size distribution* of comminuted particles in this work.

The amount of experimental data sets collected in this study is not necessarily abundant. However, for process engineering like comminution, it takes a large amount of costs to obtain even one data set that corresponds to one comminution test, including source material procurement and sorting, sample preparation, operation safety inspection, engineer labor, equipment configuration and maintenance, and data characterization. Due to these factors, data sparsity is and will still be a challenge for the development of data-driven biomass preprocessing analysis tools.

3. Numerical methods

This section describes the PBM model and the deep learning-based DNO+ model for predicting the particle size distribution of comminuted biomass in a production-scale knife mill. These models were implemented in a Python code framework and calibrated based on the reference data (either physical or numerical), as shown in Fig. 3. The PBM model was implemented as the baseline model to demonstrate its functionality as well as the known limitations. The DNO+ model was constructed to account for moisture content of the feed material as an extra input parameter for enhanced accuracy. As a data-driven model, DNO+ requires an adequate amount of data for training to achieve accuracy. Thus, in addition to the available (but limited) experimental data, tuned PBM prediction results were used as supplementary data for extended training of the DNO+ model. Although knife mill is the first milling mechanism investigated and implemented in this productionscale mill predictive model code framework, it is designed to easily to include other types of mill such as hammer mill [37] and rotary shear mill [54]. Common input parameters include the particle size distribution of feed material, moisture content, blade tip speed, and discharge screen size. Common target predictive metrics include but may not be limited to the particle size distribution of comminuted material with regard to cumulative mass.

3.1. Population balance model

The principle of population balance model is based on the integration of multiphysics events through empirical formulas, probability

theories, and systematic constraints. This section briefly describes the underlying mechanism of population balance model by using the prediction of the particle size distribution of comminuted corn stalks as an example. A schematic of the PBM model corresponding to the example is displayed in Fig. 4, showing the steps of calculations in the PBM model in consistency with the physical process.

The required input variables to initiate the PBM model workflow include a vector for mass percentage distribution, $\boldsymbol{p}_{\text{in}}\text{, corresponding}$ to a vector for particle size sequence of feed corn stalk segments, x. A profile for \mathbf{p}_{in} versus \mathbf{x} , or equivalently, cumulative mass percentage distribution, $\boldsymbol{\Phi}_{in}$, versus \mathbf{x} , describes the particle size distribution of feed material. The size for these vectors is n. This corresponds to material feeding into a mill in the physical test. The vector x does not change through the PBM calculation process and is supposed to have sufficient resolution of particle size intervals (i.e., sufficient large n) to capture the reduced particle sizes after milling. During the breakage stage, p_{in} is processed by a breakage matrix, X, to result in impacted particles in the mill chamber after a number of impacts, which is represented by a vector $\mathbf{m}^{(k)}$ for the mass percentage distribution of impacted particles after kth impact. In the classification stage, the vector $\mathbf{m}^{(k)}$ is processed with a classification matrix, C, which considers the effect of discharge screen size and the passing efficiency with empirical formulas. Particles smaller than the discharge screen size can pass through the screen with a certain passing ratio of mass and accumulate in a collection bin. In the meantime, the remainder particles in the mill chamber, which is represented by a vector for the mass percentage distribution, r, are subjected to continued grinding.

The event of particle breakage in the PBM model refers to how a group of particulates with an initial particle size distribution break in response to a single impact, depending on their inherent properties and the external impact energy. The process of particle breakage can be described by a probability function and a breakage function. The probability of a group of particulates with initial particle size sequence \mathbf{x} that break into smaller fragments under a given level of impact energy is denoted by a vector \mathbf{S} , in which each entry $S_i^{(k)}$ can be described with a master curve [55] as follows,

$$S_{i}^{(k)} = 1 - e^{(-f_{\text{res}} \cdot k \cdot (x_{i} \cdot w_{\text{kin}} - x_{i} \cdot w_{\text{min},i}))}.$$
 (2)

In Eq. (2), $f_{\rm res}$ represents the material's resistance to breaking under the impact energy, k means the kth impact between mill knife and biomass particle, x_i is the ith entry in ${\bf x}$, $w_{\rm kin}$ is the impact specific kinetic energy, and $w_{\rm min}$ is the minimum specific energy required for breakage. Among those parameters, $w_{\rm kin}$ can be estimated with $v^2/2$, where v is the linear velocity of the mill blade tip. The parameters $f_{\rm res}$ and $w_{\rm min}$ can vary upon other factors such as particle morphology and material properties, and thus cannot be accurately determined from a priori calculation or measurement. These two parameters are usually unknown for a material that has not been studied previously and must be determined by other approaches such as data fitting, which will be described later.

The breakage function matrix $\boldsymbol{B}^{(k)}$ with size of $n \times n$ describes the particle population resulted from the breakage of primary particles into secondary particles after kth impact. $\boldsymbol{B}^{(k)}$ is a lower triangular matrix and each entry $\boldsymbol{B}^{(k)}_{i,j}$ can be expressed as [33],

$$B_{i,j}^{(k)} = \begin{cases} 0 & , & i < j \\ 1 & , & i = j \\ \frac{1}{2} \left[1 + \tanh\left(\frac{x_{i} - x_{\min}}{x_{\min}}\right) \right] \cdot \left(\frac{\mathbf{x}_{j}}{\mathbf{x}_{i}}\right)^{q} & , & i > j \end{cases}$$
 (3)

with

$$q = -\frac{\gamma}{(k \cdot x_j \cdot w_{\rm kin})^{\alpha}} \left(v - \frac{(k \cdot x_j \cdot w_{\rm kin})^{\alpha}}{\gamma} d \right),\tag{4}$$

where x_{\min} is the predefined minimum particle size, and q is the exponent of the heuristic power law approximated by a linear function of the impact velocity v [33]. The parameters γ and α are material

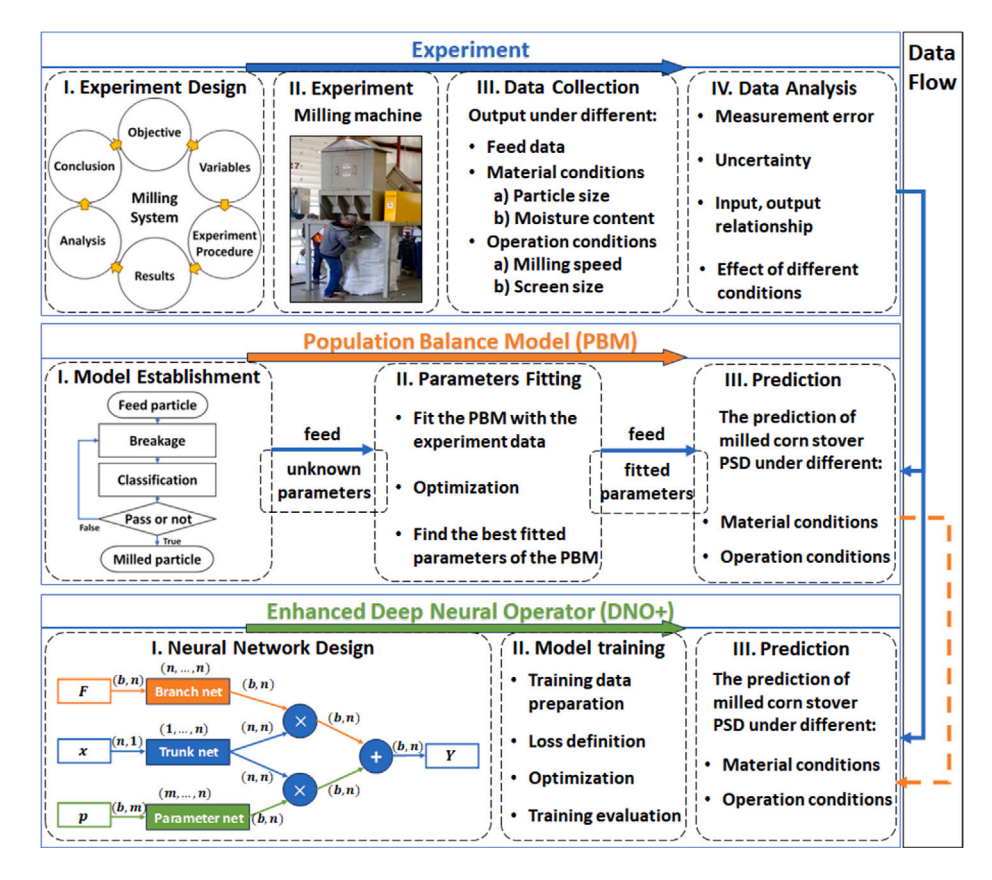


Fig. 3. Schematic of a unified framework for predicting biomass comminution. The population balance model predicts the particle size distribution of comminuted biomass and provides extra data to support the training of deep learning models. A data-driven model, enhanced deep neural operator (DNO+), is proposed and considers additional material properties.

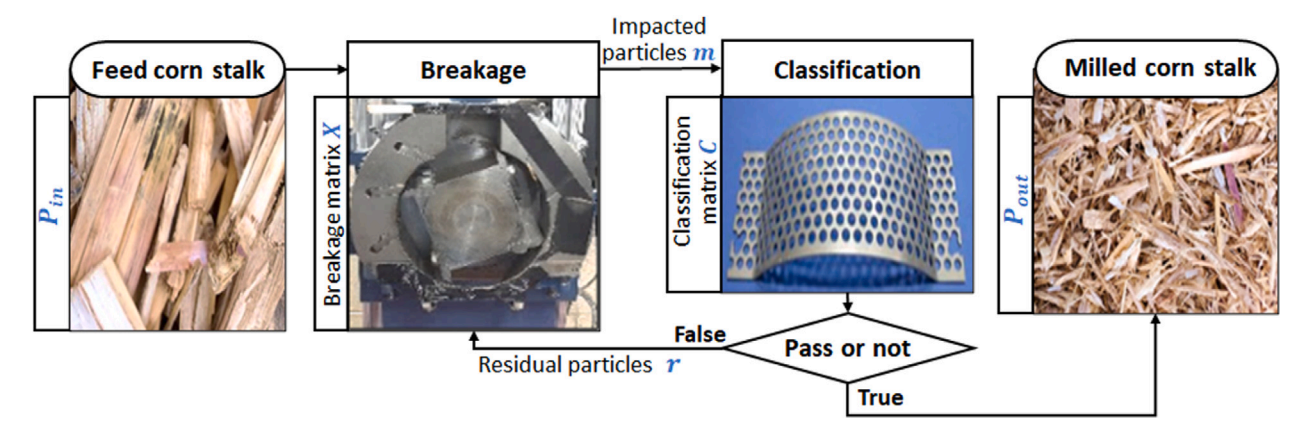


Fig. 4. Schematic of the PBM process for corn stover milling machine. According to the sequence of experiments, PBM calculates the stages of corn stover feeding, breakage, classification, and recycling through the concept of probability, and draws the final prediction results.

properties for breakage function characterization and d is a constant parameter, which can be set as fitting parameters.

The breakage matrix $\boldsymbol{X}^{(k)}$ with size of $n \times n$ determines the transformation of particles before and after the kth impact. $\boldsymbol{X}^{(k)}$ is a lower triangular matrix defined as

$$X_{i,j}^{(k)} = \begin{cases} 0 & , & i < j \\ 1 - S_i^{(k)} & , & i = j \\ b_{i,j}^{(k)} \cdot S_i^{(k)} & , & i > j \end{cases}$$
 (5)

where the diagonal element $X_{i,i}^{(k)}=1-S_i^{(k)}$ stands for the percentage of unbroken particles after kth impact. $X_{i-1,j}^{(k)}$ is the fraction of particles

generated by the breakage of primary particles $X_{i,j}$. $b_{i,j}^{(k)}$ is the percentage of secondary particles in the ith size entry generated from primary particles of the jth size entry, which can be expressed as,

$$b_{i,j}^{(k)} = \begin{cases} 0 & , & i \le j \\ B_{i+1,j}^{(k)} - B_{i,j}^{(k)} & , & i > j \end{cases}$$
 (6)

The impacted particles, represented by $\mathbf{m}^{(k)}$, is obtained by

$$\mathbf{m}^{(k)} = \begin{cases} \boldsymbol{X}^{(k)} \cdot \mathbf{p}_{\text{in}} &, & k = 1\\ \boldsymbol{X}^{(k)} \cdot \mathbf{r}^{(k)} &, & k > 1 \end{cases}$$
(7)

After the first impact (k=1), $\mathbf{m}^{(1)}$ is calculated from the breakage of the mass percentage of feed particles $\mathbf{p}_{\rm in}$. Particles smaller than the discharge screen size pass through the screen due to gravity and

mechanical vibration and become part of the vector \mathbf{p}_{out} for the mass percentage of discharged particles. The remainder particles in mill chamber are represented by the vector $\mathbf{r}^{(1)}$ for their mass percentage and will undergo the following impact cycle, i.e., the following PBM calculation cycle.

In reality, even when a particle becomes small enough to pass through the discharge screen, it may not go through immediately but will remain in mill chamber for extended time. Factors such as particle orientations and motions and intergranular collisions can affect the probability of small particles passing through the discharge screen. The probability of this screening process is characterized by a classification matrix, C, which depends on the ratio between the particle size and screen size, $\mathbf{x}/d_{\mathrm{scr}}$. C is a diagonal matrix with diagonal elements $C_{i,i}$ expressed as.

$$C_{i,i} = 1 - (x_i/d_{\text{scr}})^2 \cdot \tanh\left(\frac{x_i/d_{\text{scr}} - 0.02}{0.02}\right).$$
 (8)

Under the influence of the classification matrix C, the vector for mass percentage of kth discharged particles, $\mathbf{p}_{\text{out}}^{(k)}$, and the vector for mass fraction of kth post-screening remainder particles in mill chamber, $\mathbf{r}^{(k)}$, are calculated as.

$$\mathbf{p}_{\text{out}}^{(k)} = \mathbf{C} \cdot \mathbf{m}^{(k)} \tag{9}$$

and

$$\mathbf{r}^{(k)} = (I - \mathbf{C}) \cdot \mathbf{m}^{(k)}. \tag{10}$$

The vector for mass percentage of all comminuted particles, \mathbf{p}_{out} , is calculated as.

$$\mathbf{p}_{\text{out}} = C \cdot \left(X^{(1)} \cdot \mathbf{p}_{\text{in}} + \sum_{k=2}^{\infty} X^{(k)} \cdot \mathbf{r}^{(k-1)} \right). \tag{11}$$

The particle size distribution of comminuted particles refers to the range in x that corresponds to the effective range in p_{out} , i.e., the range between the first value below 1 and the last value above 0 in p_{out} .

The five parameters that appear in the above calculations, $f_{\rm res}$, $w_{\rm min}$, γ , α , and d, are related to feedstock material properties and priori unknown for a material that has not been previously studied. These parameters can be determined by fitting the PBM calculation results to the experimental data. As $w_{\rm min}$ is related to particle size, the term $x_i \cdot w_{\rm min,i}$ in Eq. (2) is assumed to be a constant, $\mathbf{x} \cdot \mathbf{w}_{\rm min}^T/n$, for a specific material. If $\mathbf{f}_{\rm N}$ is used to represent the set of fitting parameters as,

$$\mathbf{f}_{\mathrm{N}} = \left(f_{\mathrm{res}}, \frac{\mathbf{x} \cdot \mathbf{w}_{\min}^{\mathrm{T}}}{n}, \gamma, \alpha, \frac{-\gamma}{(k \cdot x_{i} \cdot w_{\mathrm{kin}})^{\alpha} \cdot d} \right) = \left(f_{\mathrm{res}}, \frac{\mathbf{x} \cdot \mathbf{w}_{\min}^{\mathrm{T}}}{n}, \gamma, \alpha, \frac{c}{d} \right),$$
(12)

where the fifth parameter is denoted c/d for simplicity and each of the five parameters is set to be in a range between 0 and 1. The objective is to minimize the difference between the experiment output $\mathbf{p}_{\text{out}}^{\text{Exp}}(\mathbf{x})$ and the PBM output $\mathbf{p}_{\text{out}}^{\text{PBM}}(\mathbf{x}, \mathbf{f}_{\text{N}})$ with \mathbf{f}_{N} . An objective function is written as,

$$\min \left\{ \sum_{i=1}^{n} ||p_{\text{out},i}^{\text{PBM}}(x_i, \mathbf{f}_{\text{N}}) - p_{\text{out},i}^{\text{Exp}}(x_i)||_2 \right\}$$

$$s.t. \ \mathbf{f}_{\text{N}} \in (0, 1).$$
(13)

When the fitting parameters are determined, the PBM model can be used to predict the particle size distribution of comminuted material. A PBM model based on the probability and empirical formula is numerically stable. An example of PBM calculations is provided in Supplementary Information A for reference.

Despite the relative simplicity of PBM in its formulation and implementation, one must be aware of a few assumptions and limitations of PBM when applying to a milling system. First, the influence of interparticle collisions and particle–boundary collisions on the resultant particle size distribution of comminuted material is assumed negligible, where the boundary refers to mill chamber casing, mill shaft and

blades. and discharge screen. Second, the milling system is assumed to operate in a stable condition, where the empirical formulas and the classification efficiency are considered valid and constant during the operation. Thus, the use of PBM ignores any possible abnormal operating conditions or stochastic events in reality that are likely to lead to unexpected particle size distribution results of comminuted material. Third, the original applications of PBM to the comminution of conventional bulk solids such as rock granules do not require considering the influence of moisture and thus moisture content of a material is not in the formulation of PBM at all. However, moisture content is a critical material attribute in biomass and has a profound influence on preprocessing, handling, and conversion. A change of moisture content in biomass feedstocks indicates the need to change the parameter \mathbf{f}_N in Eq. (13), which requires new experimental data for re-calibrating \mathbf{f}_N . Moreover, moisture content does not only affect \mathbf{f}_N but also the classification efficiency and other mechanisms in the milling process. To overcome some of the limitations of PBM for biomass comminution, data-driven approaches were proposed, which can search for the relationships between the inputs (material attributes, mill operating conditions, etc.) and outputs (e.g., particle size distribution of comminuted material) from a wider and higher dimensional space. A deep learning model is a potential candidate to start with for this development eventually toward a surrogate model of the milling process.

3.2. Enhanced deep neural operator (DNO+)

The DNO+ model does not only aim to find the operator between the input and output of a system like the standard deep neural operator but also allows for including new variables which influence the outcome of the system. The feasibility of DNO+ is derived from the universal approximation theorem.

The universal approximation theorem for operator [56] states that suppose $K_1 \subset X$, $K_2 \subset \mathbb{R}^d$ are two compact sets in Banach space X and \mathbb{R}^d , respectively. V is a compact set in $C(K_1)$ which is a Banach space of all continuous functions defined on K_1 with $\|f\|_{C(K_1)} = \max_{x \subset K} |f(x)|$. σ is a continuous non-polynomial function. G is a nonlinear continuous operator to map V into $C(K_2)$. For any $\epsilon > 0$, there are positive integers n, p, m, and constants c_i^k , ξ_k^i , θ_i^k , $\zeta_k \in \mathbb{R}^d$, $x_i \in K_1$, such that

$$|G(u)(y) - \sum_{k=1}^{p} \sum_{i=1}^{n} c_i^k \sigma(\sum_{j=1}^{m} \xi_{ij}^k u(x_j) + \theta_i^k) \cdot \underbrace{\sigma(w_k \cdot y + \zeta_k)}_{\text{trunk}}| < \varepsilon, \tag{14}$$

which holds for all $u \in V$ and $y \in K_2$. It was then developed as a generalized universal approximation theorem for operator [46] and can be expressed as,

$$|G(u)(y) - \langle \underbrace{g(u(x_1), u(x_2), \dots, u(x_m))}_{\text{branch}}, \underbrace{f(y)}_{\text{trunk}} \rangle| < \epsilon, \tag{15}$$

where g and f are continuous vector functions that can be chosen as diverse classes of neural networks. $x_1, x_2, \ldots, x_m \in K_1$. $\langle \cdot, \cdot \rangle$ denotes the dot product.

Let us assume that the operator of the response of an ideal system to inputs can be described by G(u)(y), and the disturbance factors that influence the response of the system can be expressed by another operator, F(u')(y). Then, the system response to inputs and disturbance factors can be represented by the combination of two operators H = G(u)(y) + F(u')(y). Subsequently, Eq. (15) can be simplified to express the two operators,

$$|G(u)(y) - \langle g(u(x)), f(y) \rangle| < \epsilon_1 \tag{16}$$

and

$$|F(u')(y) - \langle g'(u'(x)), f(y) \rangle| < \epsilon_2. \tag{17}$$

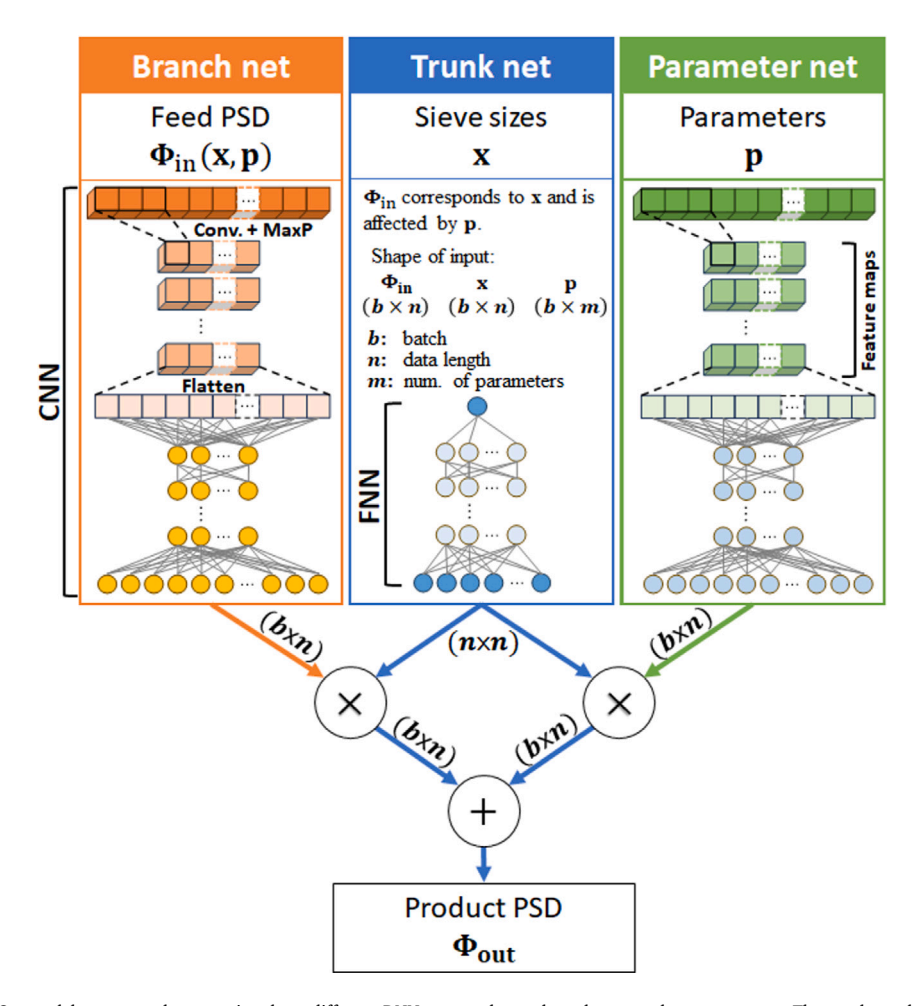


Fig. 5. A diagram of the DNO+ model structure that contains three different DNNs — trunk net, branch net, and parameter net. The trunk net handles the sieve size that runs through the system. The branch net processes the cumulative mass corresponding to the sieve size. The parameter network processes the influence of the material properties and operating conditions on the system.

According to the triangle inequality, the combination of Eqs. (16) and (17) can be expressed as,

$$|H - \langle g(u(x)), f(y) \rangle - \langle g'(u'(x)), f(y) \rangle| < \epsilon_3, \tag{18}$$

where $\epsilon_3 = \epsilon_1 + \epsilon_2$.

The DNO+ model is established based on Eq. (18), which consists of a trunk net, a branch net, and a parameter net, shown in Fig. 5. The trunk network handles an independent variable x that consistently traverses the system; the branch network processes the dependent variables that vary with x; the parameter network processes the uncertain influencing parameters p. In the implementation of DNO+ for biomass comminution, the trunk net handles the particle size sequence through the entire comminution process; the branch network processes the cumulative mass distribution with reference to the particle size sequence; the parameter network essentially correlates the impact of important material attributes (e.g., feed moisture content) and processing parameters (e.g., discharge screening size and blade tip speed) on the resultant particle size distribution of comminuted material.

The trunk network is a fully connected neural network (FNN) that processes each input feature independently. As a fundamental type of neural network architecture, the FNN consists of multiple layers of interconnected nodes. The FNN with L layers can be written as,

$$\mathcal{F}(x) = u^{(L)}(\cdots(\phi u^{(3)}(\phi u^{(2)}(\phi u^{(1)}(x))))),\tag{19}$$

where $u^{(i)}=w^{(i)}x+b^{(i)}$, the superscript (i) represents the ith layer of the neural network, $w^{(i)}$ and $b^{(i)}$ are hyperparameters. x is the input, and ϕ is the activation function. The FNN is suitable for tasks that require

preserving the order of input features, such as working with sequence data or tabular data. This allows for the FNN to effectively capture and model the sequential or structured relationships among the variables.

The branch network and parameter network are convolutional neural networks (CNNs) that can process and extract features from spatially structured data by virtue of their shared-weight architecture, wherein the convolution kernels slide across input features and yield translation-equivariant responses. Typically, CNN consists of convolutional layers, pooling layers (e.g., Max pooling in this work), and fully connected layers. A one-dimension convolution can be expressed as,

$$c = \phi(f * x + b), \tag{20}$$

where, (*) is the convolution operator. The ith value of the convolution term can be written as,

$$(f * x)[i] = \sum_{j=1}^{N} x[j] \cdot f[i-j], \tag{21}$$

where f is the filter weight, N is the length of the data sequence. The Max pooling layer reduces the spatial dimensions of the input data, while retaining the most significant features. The Max pooling takes the maximum value from the window, reducing the spatial dimensions while emphasizing the most prominent features. The operation can be represented as,

$$y[i] = \max\{c[j] : j \in n\},$$
 (22)

where *y* is the pooled output vector, $n = [i \cdot s, i \cdot s + 1, i \cdot s + 2, \cdot s, i \cdot s + w - 1],$ *s* is the stride, and *w* is the window size. The results after pooling layer

are then connected to the fully connected layers, and the entire CNN can be written as,

$$\mathscr{C}(x) = \mathscr{F}(y(x)). \tag{23}$$

In the implementation of the DNO+ model for biomass comminution, the primary input of the model is the feed cumulative mass distribution $\boldsymbol{\Phi}_{\text{in}}$ with reference to particle size sequence \mathbf{x} , plus the influence factors \mathbf{p} to the system. The cumulative discharge mass $\boldsymbol{\Phi}_{\text{out}}$ can be expressed as,

$$\boldsymbol{\Phi}_{\text{out}} = \mathcal{C}(\boldsymbol{\Phi}_{\text{in}}) \cdot \mathcal{F}(\mathbf{x}) + \mathcal{C}(\mathbf{p}) \cdot \mathcal{F}(\mathbf{x}). \tag{24}$$

By introducing the additional parameter network, the DNO+ model can construct the relationship between the input and output of a system with growing complexity.

4. Results and discussions

Based on the experimental data obtained in the test of corn stalk milling using the JRS knife mill, this section reports and analyzes the influence of moisture content, blade tip speed, and discharge screen size on the particle size distribution of comminuted material. The performance of the PBM and DNO+ models for predicting the corresponding process is also presented and evaluated.

4.1. Experiment results and analysis

The sorted corn stalks were served as the input biomass fed into the JRS knife mill. The impact of moisture content of corn stalks, discharge screen size, and blade tip speed was considered, respectively, on the experimental results. The resultant particle size distribution of comminuted material in each test was measured three times to determine the mean (μ) and standard deviation (σ). Typically, for a normal distribution, 95% of the data fell within approximately 1.96 standard deviations of the mean. Therefore, a 95% confidence interval is often constructed using the formula:

$$CI = \mu \pm 1.96\sigma. \tag{25}$$

A 95% confidence interval of particle size distribution is constructed using the upper bound of $\mu + 1.96\sigma$ and the lower bound of $\mu - 1.96\sigma$. In this paper, the particle size distribution of comminuted material is represented corresponding to the cumulative mass percentage (0 – 100%).

First, the influence of feed moisture content on the comminution outcome with a fixed blade tip speed and discharge screen was investigated. Two motor output frequencies of 60 Hz and 40 Hz were used, respectively, corresponding to the full (9.8 m s⁻¹ blade tip speed) and reduced power (6.5 m s⁻¹ blade tip speed) of the mill. The discharge screen perforation diameter is 12.7 mm. The profiles of cumulative mass percentage versus sieve size of comminuted material are shown in Fig. 6 for the settings of (9.8 m s⁻¹ blade tip speed, 12.7 mm screen size) and $(6.5 \text{ m s}^{-1} \text{ blade tip speed}, 12.7 \text{ mm screen size})$, respectively. Under each setting, a medium moisture content of 20% and a high moisture content of 40% were chosen, which are within the typical ranges of moisture content of corn stover feedstocks in the U.S. Midwest and South. These tests allowed for investigating the influence of the processing parameters and material attributes on the particle size distribution of comminuted corn stalks. Observed in Fig. 6, there is a distinct gap between the 95% confidence interval boundaries of the profiles for the case of 20% moisture content and the case of 40% moisture content, which indicates a measurable influence of moisture content on the resultant particle size distribution of comminuted particles. Fig. 6 also shows that a higher moisture content in feed corn stalks resulted in larger sizes of the comminuted particles (though not necessarily wider size distributions). Though seeking a scientific understanding of the relationship between the feed moisture content and the particle size distribution of comminuted particles is beyond the work scope, it is

worth noting that the change of moisture content in corn stalks alters their mechanical properties, which consequently affects the outcome of the collisions between the particles and knife blades as well as the dynamics of the particles in the mill chamber.

Second, the influence of blade tip speed on the particle size distribution of comminuted material with a fixed feed moisture content and discharge screen was investigated. Two discharge screens with perforation diameters of 12.7 mm and 19.05 mm, respectively, were used. In this study, the feed corn stalks with a fixed moisture content of 40% were used. The profiles of cumulative mass percentage versus sieve size of comminuted particles with the 95% confidence bandwidths are shown in Fig. 7 for the settings of (40% moisture content, 12.7 mm screen size) and (40% moisture content, 19.05 mm screen size), respectively. Under each setting, three blade tip speeds, 9.8 m s⁻¹, 8.2 m s⁻¹, and 6.5 m s⁻¹, were selected respectively, resulting in three profiles. Fig. 7a shows that with the setting of (40% moisture content, 12.7 mm discharge screen size), the three profiles partially overlap with each other over the entire size range. In contrast, Fig. 7b shows that with the setting of (40% moisture content, 19.05 mm discharge screen size), the overlap between the three profiles is even more pronounced. These results suggest that the particle size distribution of comminuted corn stalk particles produced by the JRS knife mill is relatively insensitive to the change of blade tip speed in the tested range. At the lowest motor power tested (40 Hz), the energy of knife cutting is enough to sufficiently break the corn stalks. It is worth noting again that by default the JRS knife mill can only provide the 60 Hz motor power. By re-configuring the power system of the mill, the motor power was reduced. Nevertheless, the motor power cannot be arbitrarily reduced to sustain the stable mill operation. The motor power of 40 Hz is found to be the lowest to guarantee safe operation. To conclude, the balde tip speed is found not a critical processing parameter for milling corn stalks with the JRS knife mill. The JRS knife mill operating at a 33% reduction from the default power can substantially decrease the cost of energy, while producing about the same particle size distribution of comminuted corn stalks.

Finally, the influence of discharge screen size on the comminution outcome with a fixed feed moisture content and blade tip speed was investigated. Two motor frequencies of 40 Hz (6.5 m s⁻¹ blade tip speed) and 60 Hz (9.8 m $\rm s^{-1}$ blade tip speed), respectively, were used. In this study, the feed corn stalks with a fixed moisture content of 40% were used. By mill design, discharge screen size is the leading processing parameter that controls the comminution outcome. The profiles of cumulative mass percentage versus sieve size of comminuted material with the 95% confidence bandwidths are shown in Fig. 8 for the settings of (6.5 m s⁻¹ blade tip speed, 40% moisture content) and (9.8 m s⁻¹ blade tip speed, 40% moisture content), respectively. Under each setting, two screen sizes were chosen, respectively, resulting in two profiles. As expected, the two profiles are distant from each other, clearly demonstrating the criticality of discharge screen size in controlling the comminution outcome. The profile corresponding to the larger screen size (19.05 mm) resulted in a wider size distribution and larger maximum size (13-14 mm). In contrast, the profile corresponding to the smaller screen size (12.7 mm) resulted in smaller maximum size (9-10 mm). Notice that the maximum sizes in each profile are 20-30%smaller than the discharge screen sizes, which are partially attributed to the large aspect ratio of the comminuted corn stalk particles.

Based on the parametric investigations of the experimental data, moisture content of feed corn stalks and discharge screen size are found to significantly influence the comminution outcome, whereas the impact of blade tip speed is less evident. However, to save energy cost by reducing motor power of a mill with the fixed factory settings requires additional cost of technical staff for equipment maintenance. Thus, from the safe operation perspective, achieving control of biomass comminution is most feasible by choosing proper discharge screen sizes and feed moisture content.

M. Lu et al. Powder Technology 441 (2024) 119830

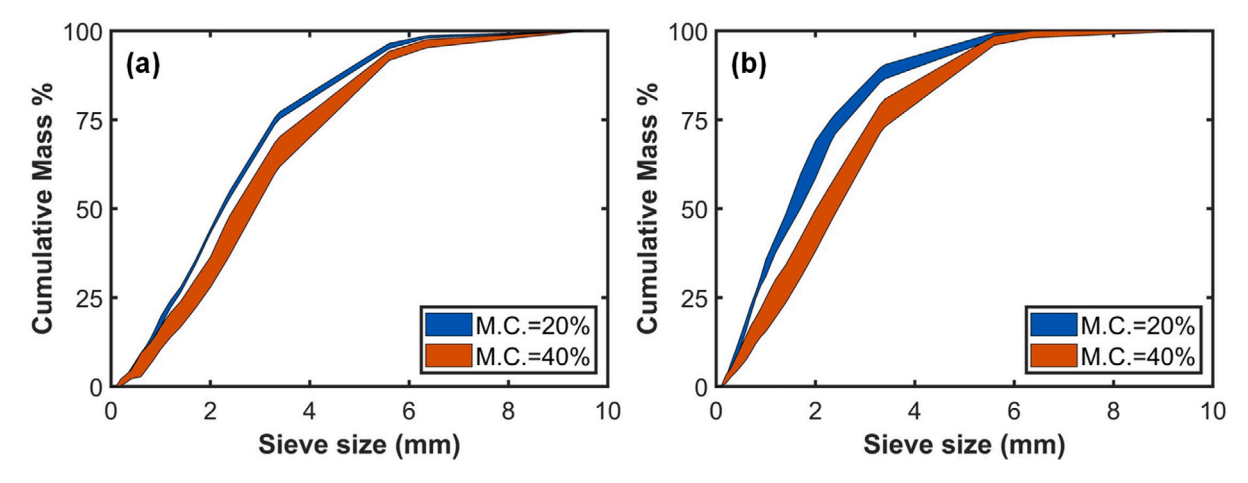


Fig. 6. Influence of two M.C. levels of feed corn stalks on the cumulative mass percentage versus milled particle sieve size with the 12.7 mm screen size, and (a) 6.5 and (b) 9.8 m s $^{-1}$ blade tip speed, respectively.

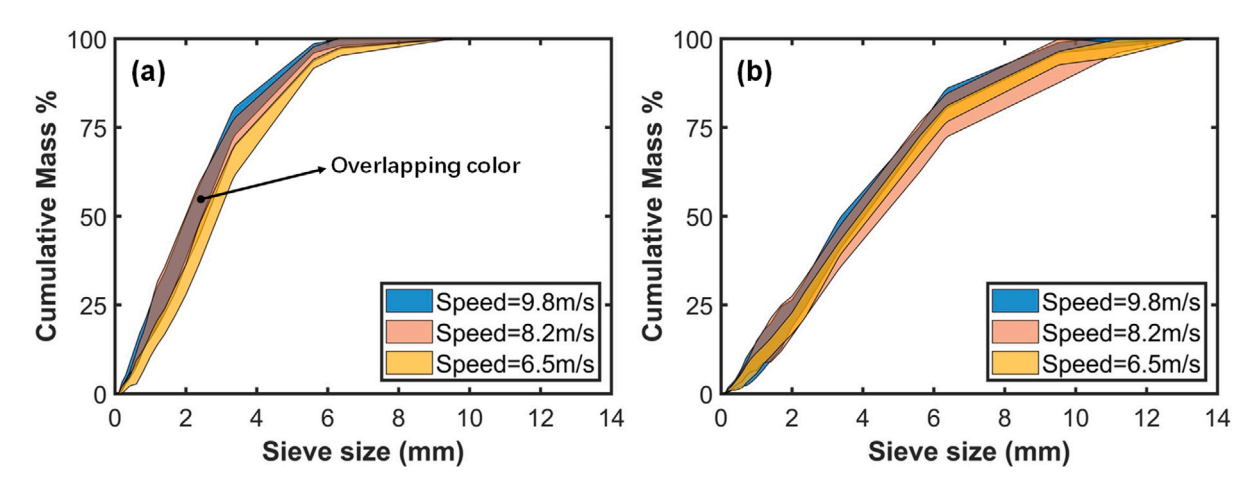


Fig. 7. Influence of three blade tip speeds on the cumulative mass percentage versus comminuted particle sieve size with the 40% M.C. in feed corn stalks, and (a) 12.7 and (b) 19.5 mm screen size, respectively.

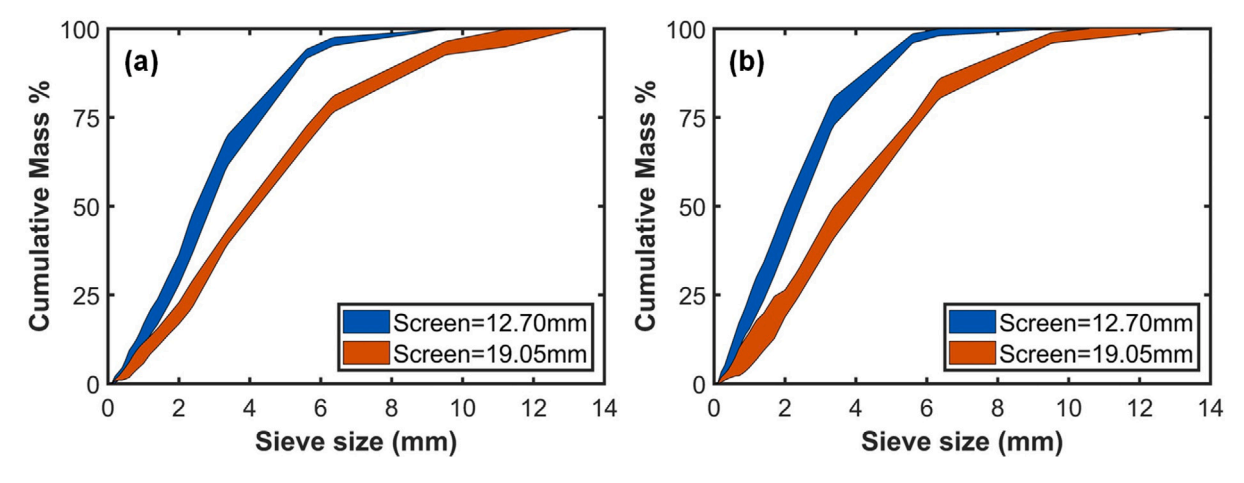


Fig. 8. Influence of two discharge screen sizes on the cumulative mass percentage versus comminuted particle sieve size with 40% M.C. in feed corn stalks, and (a) 6.5 and (b) 9.8 m s^{-1} blade tip speed, respectively.

4.2. Fitting and predictability of extended PBM

Based on the obtained experimental data, the PBM model for the JRS mill process of corn stalks was calibrated by incorporating \mathbf{f}_{N} in Eq. (12) as the unknown parameters. The objective function in

Eq. (13) was optimized using the genetic algorithm (GA) [57]. To describe the GA method briefly, it solves optimization problems through a process inspired by natural selection. In this study, a population size of 100 was set for each generation and each variable in \mathbf{f}_{rmN} is represented with 16-bit binary encoding. To begin with the calibration, the initial population was created and graded according to Eq. (13).

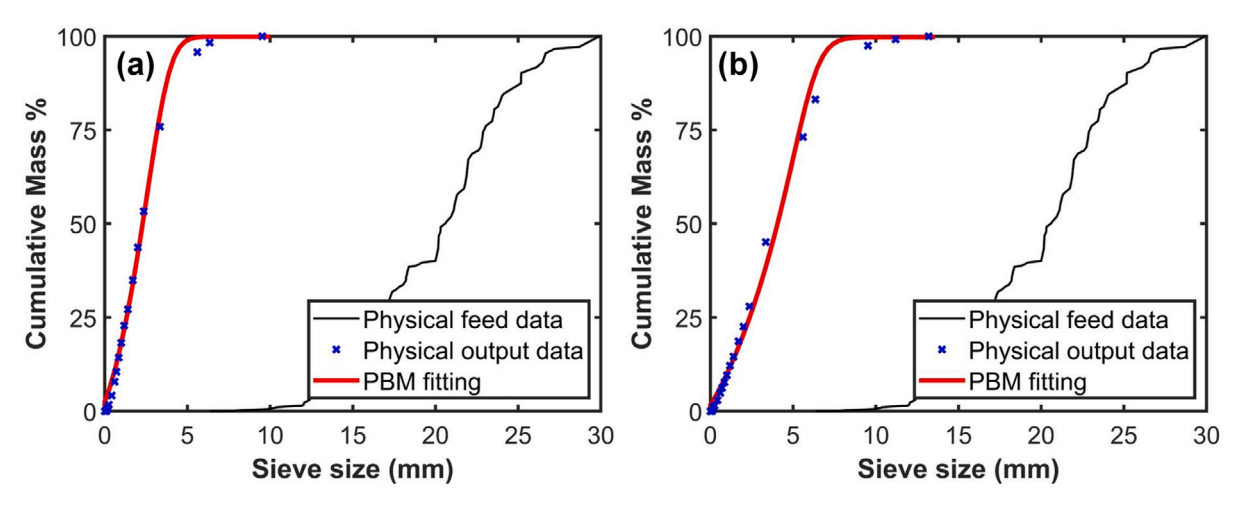


Fig. 9. Examples of the PBM fitting accuracy in two test conditions in Table 1: (a) test No. 1 (6.5 m s $^{-1}$ blade tip speed, 20% M.C. and 12.70 mm screen.). (b) test No. 12 (9.8 m s $^{-1}$ blade tip speed), 40% M.C. and 19.05 mm screen.

Table 2 The fitting parameters in \mathbf{f}_N corresponding to the list of test conditions for the JRS knife mill operation of corn stalks.

Test no.	$f_{\rm res}$	$\mathbf{x} \cdot \mathbf{w}_{\min}/n$	γ	α	c/d	R^2
1	0.3918	0.0515	0.1652	0.3811	0.8955	0.9965
2	0.2567	0.0713	0.2746	0.4060	0.8104	0.9905
3	0.4661	0.0461	0.1315	0.7891	0.1943	0.9924
4	0.1665	0.1084	0.2225	0.5189	0.5555	0.9940
5	0.6248	0.0157	0.1449	0.4937	0.8096	0.9902
6	0.0612	0.0308	0.1707	0.2337	0.8719	0.9941
7	0.1189	0.0482	0.1641	0.2942	0.7919	0.9975
8	0.1447	0.1958	0.2544	0.9922	0.4755	0.9935
9	0.6129	0.0075	0.1176	0.2837	0.5696	0.9942
10	0.9883	0.1667	0.1486	0.5232	0.4442	0.9917
11	0.2903	0.0094	0.1632	0.8088	0.3260	0.9933
12	0.0801	0.2855	0.1117	0.0666	0.4860	0.9948

The individuals from the current population who had high scores were selected as the parents for producing the children by crossover and mutation for the next generation, during which a crossover rate of 0.9 and a mutation rate of 0.05 were used. Over successive generations, the population evolved toward an optimal solution that determined \mathbf{f}_{N} . Finally, the parameters in \mathbf{f}_{N} were inserted into Eqs. (2) and (4) to complete a functioning PBM model that can be used to predict the particle size distribution of comminuted corn stalks given the reasonable inputs.

Following the calibration method described above, 12 sets of \mathbf{f}_{N} were determined, respectively, based on 12 experimental test conditions in Table 1 and their corresponding test data sets. Table 2 lists the 12 sets of \mathbf{f}_{N} and the coefficient of determination R^2 for each test condition, calculated as,

$$R^{2} = 1 - \frac{\sum_{i} (\hat{U} - U_{\text{PBM}})^{2}}{\sum_{i} (\hat{U} - \bar{U})^{2}},$$
(26)

where, \hat{U} is the experiment data, \hat{U} is the mean value of \hat{U} , and U_{PBM} stands for the PBM predictions. As shown in Table 2, the PBM predictions reached very high R^2 values (or in other words, good fitting) for all the 12 test conditions. Some representative PBM fitting results from these tests are shown in Fig. 9, demonstrating the feasibility to adapt and extend the existing PBM model for biomass comminution [36] to predict the large-scale JRS knife mill operation. More test conditions that show the PBM fitting accuracy like in Fig. 9 can be found in Supplementary Information B.

Despite the accurate fitting of the PBM prediction in each individual test condition, PBM requires re-calibration for a different set of \mathbf{f}_{N} when the feed moisture content is changed. To overcome this limitation, one

needs a mechanism that accounts for the influence of feed moisture content in the PBM model to reduce the need for the effort of re-calibrating or choosing different \mathbf{f}_N , for using the PBM model given different feed moisture content. In this work, a novel method is introduced to incorporate feed moisture content into the PBM calculations by using the process of random forest regression (RFR) [58,59]. The RFR process established correlations (or specifically, a mapping operator) from feed moisture content and discharge screen size to the determined f_N in Table 2. To articulate this procedure by example, part of the sets of \mathbf{f}_{N} (No. 1, 2, 5, 6, and 9–12) in Table 2 were chosen for training the RFR process and generating the mapping operator, as the test conditions corresponding to these sets of f_N involved the minimum and maximum values of the input parameters. Given the input parameters (i.e., blade tip speed, feed moisture content, and discharge screen size), the resultant mapping operator can calculate a set of \mathbf{f}_N in the intrinsic workflow of PBM, instead of requiring it as part of the input. This reduces the reliance of the PBM model on predetermined \mathbf{f}_{N} and significantly improves the applicability of the model.

After the mapping operator was generated, two sources of reference data were used respectively: (1) experimental data of the No. 3, 4, 7, and 8 test conditions in Table 1, and (2) PBM predictions for conditions that use the No. 1, 2, 5, 6, 9–12 sets of $\mathbf{f}_{\rm N}$ in Table 2, to assess the PBM predictions that used the mapping operator. For an individual test case, the L^2 norm is used to represent the relative error (ε) regarding the reference data:

$$\varepsilon = \frac{1}{n} \| (\boldsymbol{\Phi}_{\text{out}}^{\text{ref}} - \boldsymbol{\Phi}_{\text{out}}^{\text{pred}}) / \boldsymbol{\Phi}_{\text{out}}^{\text{ref}} \|_{2} \times 100\%, \tag{27}$$

where n is the number of data points in the profile of cumulative mass percentage (above 0 and below 100%) versus particle size sequence. Fig. 10 displays examples of the comparative PBM predictions, showing that the PBM prediction profiles that used the mapping operator (green dash curves) agree closely with those used the individually determined groups of fitting parameters f_N (red solid curves). In the two examples in Fig. 10, the PBM predictions (green dash curves) reached a relative error of 14.13% and 10.25%, respectively, with reference to the experimental data profiles (blue cross markers). This corresponds to the prediction accuracy in 85%–93%, which is practically acceptable for biomass comminution design regarding the high variability of biomass physical properties in large bulks and hence the input parameters for PBM. More test conditions that show the comparison like in Fig. 10 can be found in Supplementary Information B.

With the extended PBM, it becomes feasible to predict the particle size distribution of JRS knife-milled biomass beyond the experimental conditions in Table 1, though within the training parameter range. The influence of the primary processing parameters (i.e., screen size

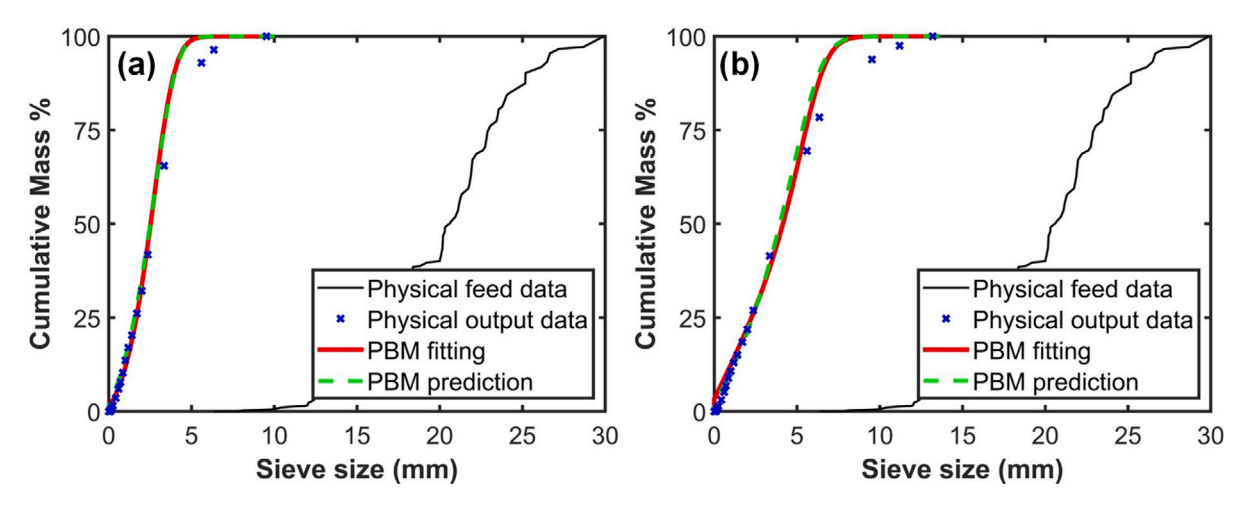


Fig. 10. Examples of comparison between PBM predictions using individually determined sets of fitting parameters (red solid curve) and PBM predictions using trained mapping operator (green dash curve) in two test conditions in Table 1: (a) test No. 3 (6.5 m s⁻¹ blade tip speed, 40% M.C. and 12.70 mm screen) (b) test No. 8 (8.2 m s⁻¹ blade tip speed, 40% M.C. and 19.05 mm screen).

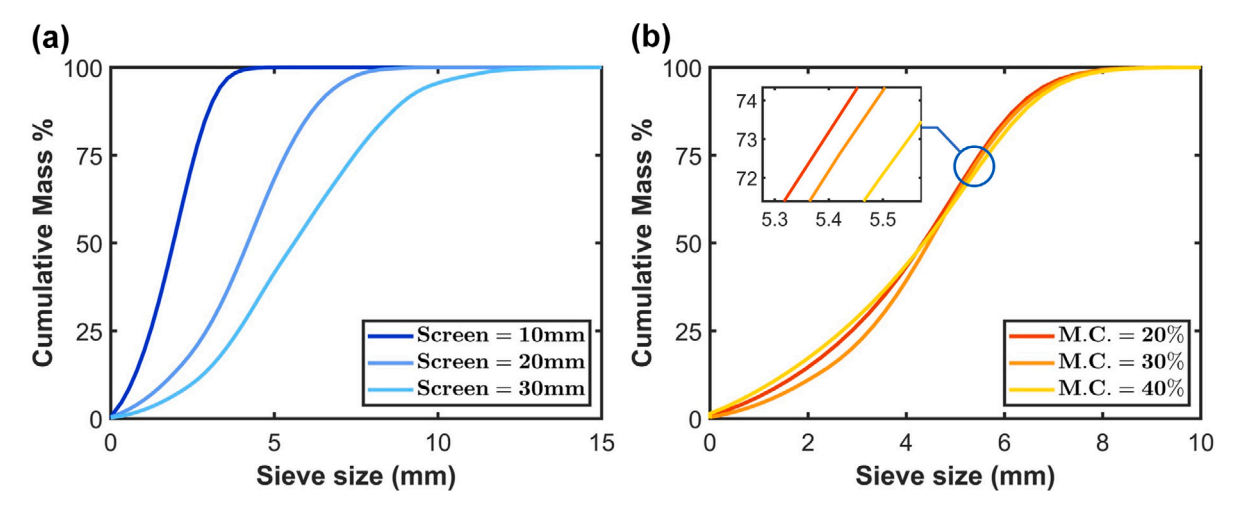


Fig. 11. Examples of influence of (a) screen size and (b) moisture content on the PBM predictions.

and moisture content) on the PBM predictions can be observed in a parametric study, as illustrated in Fig. 11. Fig. 11a depicts the variation of PBM predicted particle size distributions with screen size increasing from 10 mm to 30 mm, under a fixed moisture content of 40%. Wider particle size distribution with larger maximum particle size results from larger screen size, which is consistent with the experimental observations. Fig. 11b depicts the variation of PBM predicted particle size distribution with moisture content increasing from 20% to 40%, under a fixed screen size of 19.05 mm. When the cumulative mass is below 50%, the influence of moisture content is not monotonic. When the cumulative mass exceeds 50%, higher moisture content tends to generate slightly larger particle size, shown in the zoom-in graph in Fig. 11b. This is likely due to decreased brittleness of biomass with increasing moisture content, making it less effective to size reduce with shear cut.

4.3. Training and accuracy of DNO+

Due to the sparsity of experimental datasets for the training purpose of deep learning-based model DNO+, the extended PBM which uses the mapping operator and demonstrates satisfying predictability in Section 4.2, was used to generate the needed training datasets. The information contained in one training dataset includes distribution of feed mass versus sieve size, feed moisture content, discharge screen size, and distribution of discharged mass versus sieve size. The blade tip

speed is excluded from the DNO+ model, since the comminution outcome is found relatively insensitive to blade tip speed in the operational range, shown in Section 4.1. The training datasets were generated in an expanded input parameter space with a refined resolution. For example, the range of feed moisture content was expanded from (20%, 40%) to (10%, 50%), and the range of discharge screen size was expanded to (10 mm, 30 mm).

To determine the critical amount of datasets for training the DNO+ model, a sensitivity study ranging from 100 to 600 datasets in the expanded input parameter space was conducted to find the relationship between the relative error of the DNO+ model and the number of training datasets. Fig. 12 shows the distribution of relative errors versus the number of training datasets, where the median of the relative error decreases from 1.034% to 0.4% when the training datasets increase from 100 to 600. This has verified that the increasing training datasets in a fixed input parameter space improves the prediction accuracy of the trained DNO+ model. In the meantime, it is worth noting that though the median of the relative error in the case of 100 training datasets is only about 1%, the stability of the model prediction, indicated by the maximum relative error over 6%, is not satisfying. In contrast, when 300 or more training datasets are used, the maximum relative error drops below 3% and the 75th percentile relative error stays below 1%, indicating the least datasets to guarantee both the accuracy and stability of predictions for training the DNO+ model.

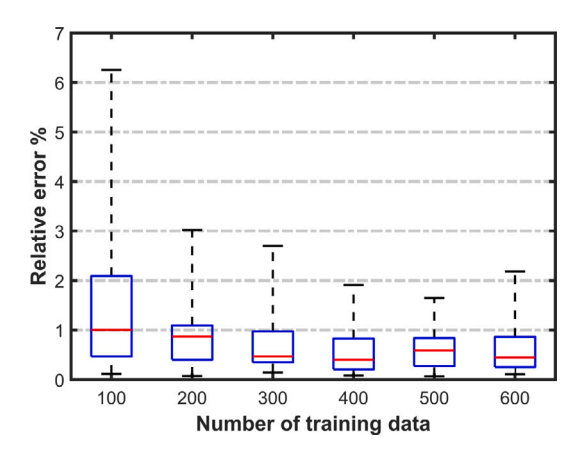


Fig. 12. Box plot of the relative error of the DNO+ model versus the number of training data sets. In each box, the center mark (red) represents the median of the relative errors of individual cases; the bottom and top edges of the box represent the 25th and 75th percentiles of the relative error; the maximum whisker length is specified as four times of the interquartile range.

Based on the critical amount of datasets suggested from the sensitivity study, 400 datasets were generated using the extended PBM, where 300 of the 400 datasets were used for training the DNO+ model. The remaining 100 datasets were used as test cases for evaluating the prediction accuracy of the trained DNO+ model. To reduce the chance of overfitting, 5% Gaussian noise was added to the original datasets to make the trained model more robust and avoid excessive reliance on input data, thus enhancing the model's general predictability. This approach is useful when dealing with small training datasets or poor source data quality. The assessment shows that the median of the total relative error of the trained DNO+ model is 0.71% for the 100 test cases, corresponding to an accuracy of 99.29%. Fig. 13 displays the results of predictions for 2 of the 100 test cases, which correspond to the experimental test No. 8 and No. 12 in Table 1. These two test cases refer to comminution with low feed moisture content and small discharge screen, and high feed moisture content and large discharge screen, respectively, which are representative of the prediction accuracy of the trained DNO+ model. In each plot of Fig. 13, the predicted profile of cumulative mass versus sieve size is compared with the reference profile, exhibiting a high degree of agreement over the entire sieve size range of discharged mass. Furthermore, Fig. 14 displays the model predictions for four test cases in the expanded and refined parameter space. In addition to the profiles of cumulative mass versus sieve size (blue lines), the profiles of distributed mass versus sieve size (red lines) are also plotted to allow for easier observation of the errors of predictions. Since the values of input feed moisture content and screen size in these test cases are outside of the original experimental test range, they are adequate examples to demonstrate the true predictability of the DNO+ model. Again, over the entire sieve size range of discharged mass, the predictions (cross markers) closely matched the reference data (solid lines) in all the four test cases, shown in Fig. 14.

To gain an in-depth understanding of the DNO+ model for engineering design applications, three particular sieve sizes, namely D10, D50, and D90, which correspond to the 10%, 50%, and 90% cumulative mass of comminuted material for the four test cases in Fig. 14, are provided in Table 3. The set of D10, D50, and D90 is a popular engineering criterion for characterizing particle size distribution in aiding the design of comminution strategies, as only three values are required. They are most suitable for hard solids and powders that do not have particle shapes of high aspect ratios (>5) such as biomass [53]. In Table 3, the magnitude of relative errors of D10, D50, and D90 is within $\pm 2\%$ in the four test cases, except for D50 in test case (c) and D10 in test case (d), which are -2.16% and -3.59%, respectively. However,

Table 3

The DNO+ model predicted D10, D50 and D90 values in the four test cases in Fig. 14.

Test case (a)	Reference	DNO+	Error	Relative error
D10	1.3207 (mm)	1.3190 (mm)	-0.0017 (mm)	-0.13%
D50	3.6774 (mm)	3.6275 (mm)	-0.0499 (mm)	-1.36%
D90	6.3869 (mm)	6.4395 (mm)	0.0526 (mm)	0.82%
Test case (b)	Reference	DNO+	Error	Relative error
D10	1.9149 (mm)	1.8981 (mm)	-0.0168 (mm)	-0.88%
D50	4.8855 (mm)	4.9787 (mm)	0.0932 (mm)	1.91%
D90	8.3252 (mm)	8.2867 (mm)	-0.0385 (mm)	-0.46%
Test case (c)	Reference	DNO+	Error	Relative error
D10	0.0006 ()	0.8385 (mm)	0.0040 (mm)	0.59%
D10	0.8336 (mm)	0.0303 (11111)	0.0049 (mm)	0.39%
D10 D50	0.8336 (mm) 2.4768 (mm)	2.4234 (mm)	-0.0534 (mm)	-2.16%
	, ,	, ,	, ,	
D50	2.4768 (mm)	2.4234 (mm)	-0.0534 (mm)	-2.16%
D50 D90	2.4768 (mm) 4.3261 (mm)	2.4234 (mm) 4.3577 (mm)	-0.0534 (mm) 0.0316 (mm)	-2.16% 0.73%
D50 D90 Test case (d)	2.4768 (mm) 4.3261 (mm) Reference	2.4234 (mm) 4.3577 (mm) DNO+	-0.0534 (mm) 0.0316 (mm) Error	-2.16% 0.73% Relative error
D50 D90 Test case (d)	2.4768 (mm) 4.3261 (mm) Reference 1.4756 (mm)	2.4234 (mm) 4.3577 (mm) DNO+ 1.4227 (mm)	-0.0534 (mm) 0.0316 (mm) Error -0.0529 (mm)	-2.16% 0.73% Relative error -3.59%

the absolute errors for D50 in test case (c) and D10 in test case (d) are only 0.0534 mm and 0.0529 mm, which are not much larger than the others. Above all, this study has proved the feasibility of developing and applying deep learning-based model DNO+ for accurately predicting biomass comminution in a production-scale mill. More importantly, the DNO+ model is capable of involving influencing factors of different data types such as the critical material attributes and mill processing parameters, which is a significant advancement over the standard DNO model that only admits the identical type of data from input to output.

5. Conclusion

Particle size distribution of lignocellulosic biomass resulted from comminution is a critical material attribute that impacts the overall productivity of biofuels or bio-based products. Predictive models for the outcome of biomass comminution based on feed material attributes and mill processing parameters are useful tools to support the design of effective biomass preprocessing. In this work, a concerted effort has been carried out to develop predictive models for biomass comminution in a large knife mill. The accomplishments and findings are summarized as follows.

- Using experimental data as the foundation for model development, a series of parametric physical tests on corn stalk comminution were conducted to determine the criticality of select feed material attributes and mill processing parameters. It is found that the moisture content of feed corn stalks and discharge screen size significantly influence the resultant particle size distribution of comminuted particles. It is also found that within the safe operational power range of the knife mill, rotor blade tip speed has little impact on the comminution outcome.
- An extended population balance model (PBM) for biomass comminution in a large knife mill has been introduced, which includes the feed moisture content as a new input parameter that is absent in the original PBM model. This is achieved by introducing the random forest regression (RFR), which establishes a mapping operator from the feed moisture content and discharge screen size to the existing groups of fitting parameters in the PBM model. Given the input parameters (moisture content, discharge screen size, blade tip speed), the mapping operator calculates a new group of fitting parameters to supply the workflow of PBM, and thus reduces the need for re-calibrating fitting parameters for different feed moisture content levels. The extended PBM model has been calibrated using the experimental data, where the PBM results match the experimental data with 99% accuracy.

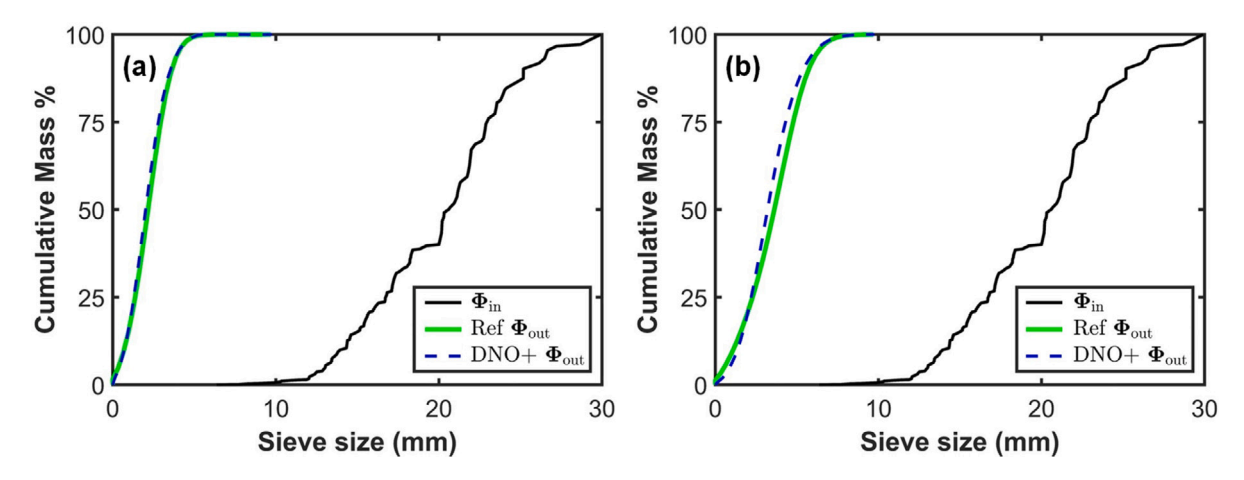


Fig. 13. Examples of DNO+ predictions (green line) for two test cases in Table 1: (a) test No. 8 (blade tip speed = 9.8 m s⁻¹, M.C. = 20%, screen size = 12.70 mm); (b) test No. 12 (blade tip speed = 9.8 m s⁻¹, M.C. = 40%, screen size = 19.05 mm). The PBM data are used as the reference Φ_{out} .

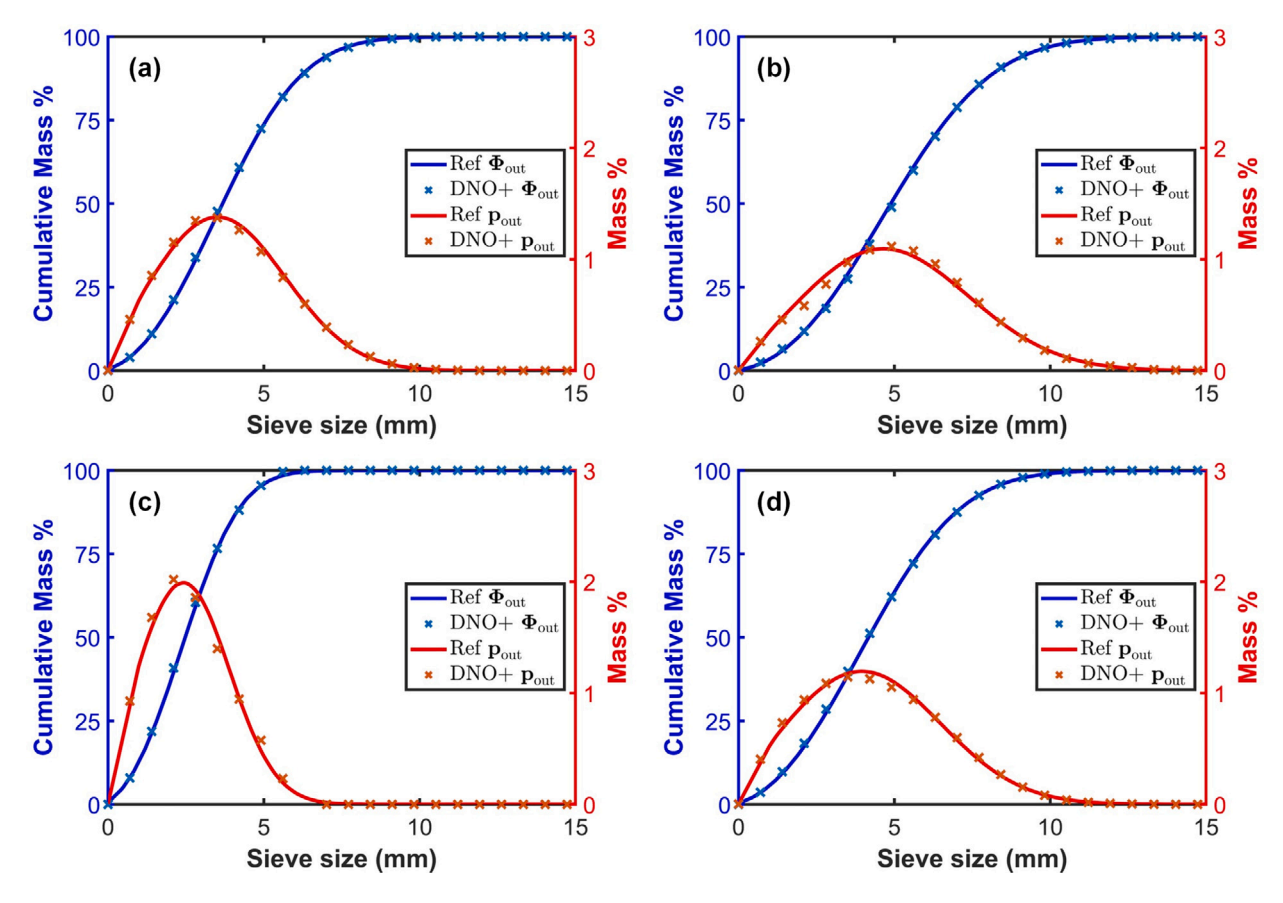


Fig. 14. Examples of DNO+ predictions (cross marker) for four test cases in the expanded and refined parameter space: (a) M.C. = 18%, screen size = 23.01 mm; (b) M.C. = 34%, screen size = 29.56 mm; (c) M.C. = 16%, screen size = 15.70 mm; (d) M.C. = 14%, screen size = 26.43 mm. The PBM data (solid line) are used as the reference.

- A deep learning-based predictive model, namely enhanced deep neural operator (DNO+), has been developed for biomass comminution. The original deep neural operator (DNO) model identifies an operator between the single type of input and output sequences of a system (e.g., feed particle size distribution versus outcome particle size distribution) and cannot involve other different types of input. In contrast, the DNO+ model can include additional types of input such as feed moisture content and discharge screen size that exert influence on the system behavior. The DNO+ model has been trained to predict corn stalk comminution in a large knife mill based on the extensive training datasets generated by the extended PBM model. A sensitivity study has
- been conducted to suggest the minimum training datasets for DNO+ to sustain consistent accuracy in the training parameter space, where the trained DNO+ model has achieved over 98% accuracy.
- Though both the extended PBM model and the DNO+ model achieved accurate predictions for biomass comminution at scale, the extension and application of DNO+ do not require strong subject matter expertise. Therefore, it would be easier to adapt the DNO+ model for other preprocessing operations with different physical mechanisms, such as air classification and separation. However, due to the expensive costs and hence sparsity of production-scale experimental data, the future development and

application of the DNO+ model in the area of biomass preprocessing will still likely rely heavily on high-quality emulated training datasets such as those generated by the PBM predictions in this work or other regression methods.

As a final word, it is straightforward to apply the extended PBM and DNO+ models to the traditional comminution of hard solids such as mineral ores and pharmaceutical intermediates. A focus of the follow-on research will be on developing efficient methods to streamline experimental data production and post-processing to support the rapid training of the DNO+ model.

CRediT authorship contribution statement

Minglei Lu: Writing – original draft, Visualization, Validation, Software, Methodology, Investigation, Formal analysis, Data curation, Conceptualization. Yidong Xia: Writing – original draft, Visualization, Validation, Supervision, Software, Resources, Project administration, Methodology, Investigation, Funding acquisition, Formal analysis, Data curation, Conceptualization. Tiasha Bhattacharjee: Software, Resources, Methodology, Data curation, Conceptualization. Jordan Klinger: Writing – original draft, Supervision, Resources, Project administration, Funding acquisition, Conceptualization. Zhen Li: Supervision, Resources, Methodology, Funding acquisition.

Declaration of competing interest

The authors declare that they have no known competing financial interests or personal relationships that could have appeared to influence the work reported in this paper.

Data availability

Data will be made available on request.

Acknowledgments

The research is primarily supported by the U.S. Department of Energy (DOE), Office of Energy Efficiency and Renewable Energy (EERE), Bioenergy Technologies Office (BETO), the Feedstock-Conversion Interface Consortium (FCIC), under DOE Idaho Operations Office with Contract No. DE-AC07-05ID14517. The research is supported in part by the DOE, EERE, BETO project entitled "Dynamic processing of biomass residues at the pilot-scale as a function of feedstock attributes using fractionation, digital twin modeling, and online sensors", under DOE Idaho Operations Office with Contract No. DE-AC07-05ID14517. The research is supported in part through the Idaho National Laboratory (INL) Laboratory Directed Research & Development (LDRD) Program under DOE Idaho Operations Office Contract DE-AC07-05ID14517. Minglei Lu are partially and Zhen Li are primarily supported by the AIM for Composites, an Energy Frontier Research Center funded by the U.S. DOE, Office of Science, USA, Basic Energy Sciences (BES), USA, under Award DE-SC0023389 and by the National Science Foundation, United States (Grants OAC-2103967 and CDS&E-2204011).

Appendix A. Supplementary data

The source code for implementing the models in this work is available at https://doi.org/10.11578/dc.20231213.2.

Supplementary Information A: This document elucidates the biomass comminution process with a simplified example.

Supplementary Information B: This document supplements the main article's discussion on PBM fitting and prediction results.

Supplementary material related to this article can be found online at https://doi.org/10.1016/j.powtec.2024.119830.

References

- S. Hernandez, T.L. Westover, A.C. Matthews, J.C.B. Ryan, C.L. Williams, Feeding properties and behavior of hammer-and knife-milled pine, Powder Technol. 320 (2017) 191–201.
- [2] Y. Sun, J. Cheng, Hydrolysis of lignocellulosic materials for ethanol production: A review, Bioresour. Technol. 83 (1) (2002) 1–11.
- [3] M.F.S. Khan, M. Akbar, Z. Xu, H. Wang, A review on the role of pretreatment technologies in the hydrolysis of lignocellulosic biomass of corn stover, Biomass Bioenergy 155 (2021) 106276.
- [4] W. Jin, J.J. Stickel, Y. Xia, J. Klinger, A review of computational models for the flow of milled biomass part II: Continuum-mechanics models, ACS Sustain. Chem. Eng. 8 (16) (2020) 6157–6172.
- [5] P. Cleary, Modelling comminution devices using DEM, Int. J. Numer. Anal. Methods Geomech. 25 (1) (2001) 83–105.
- [6] M.S. Powell, R.D. Morrison, The future of comminution modelling, Int. J. Miner. Process. 84 (1–4) (2007) 228–239.
- [7] H. Mio, J. Kano, F. Saito, Scale-up method of planetary ball mill, Chem. Eng. Sci. 59 (24) (2004) 5909–5916.
- [8] M. Khanal, W. Schubert, J. Tomas, Discrete element method simulation of bed comminution, Min. Eng. 20 (2) (2007) 179–187.
- [9] N. Djordjevic, F.N. Shi, R.D. Morrison, Applying discrete element modelling to vertical and horizontal shaft impact crushers, Min. Eng. 16 (10) (2003) 983–991.
- [10] C.C. Kwan, H. Mio, Y.Q. Chen, Y.L. Ding, F. Saito, D.G. Papadopoulos, A.C. Bentham, M. Ghadiri, Analysis of the milling rate of pharmaceutical powders using the Distinct Element Method (DEM), Chem. Eng. Sci. 60 (5) (2005) 1441–1448.
- [11] S. Naik, R. Malla, M. Shaw, B. Chaudhuri, Investigation of comminution in a Wiley Mill: Experiments and DEM Simulations, Powder Technol. 237 (2013) 338–354
- [12] M. Yang, C. Li, Z. Said, Y. Zhang, R. Li, S. Debnath, H.M. Ali, T. Gao, Y. Long, Semiempirical heat flux model of hard-brittle bone material in ductile microgrinding. J. Manuf. Process. 71 (2021) 501–514.
- [13] N.S. Weerasekara, M.S. Powell, P.W. Cleary, L.M. Tavares, M. Evertsson, R.D. Morrison, J. Quist, R.M. Carvalho, The contribution of DEM to the science of comminution, Powder Technol. 248 (2013) 3–24.
- [14] C. Thornton, K.K. Yin, M.J. Adams, Numerical simulation of the impact fracture and fragmentation of agglomerates, J. Phys. D: Appl. Phys. 29 (2) (1996) 424.
- [15] C. Thornton, M.T. Ciomocos, M.J. Adams, Numerical simulations of agglomerate impact breakage, Powder Technol. 105 (1–3) (1999) 74–82.
- [16] M. Khanal, R. Raghuramakrishnan, J. Tomas, Discrete element method simulation of effect of aggregate shape on fragmentation of particle composite, Chem. Eng. Technol.: Ind. Chem.-Plant Equip.-Process Eng.-Biotechnol. 31 (10) (2008) 1526–1531.
- [17] G.M. Campbell, P.J. Bunn, C. Webb, S.C.W. Hook, On predicting roller milling performance: Part II. The breakage function, Powder Technol. 115 (3) (2001) 243–255.
- [18] Y. Xia, J.J. Stickel, W. Jin, J. Klinger, A review of computational models for the flow of milled biomass part I: discrete-particle models, ACS Sustain. Chem. Eng. 8 (16) (2020) 6142–6156.
- [19] Y. Guo, C. Wassgren, B. Hancock, W. Ketterhagen, J. Curtis, Computational study of granular shear flows of dry flexible fibres using the discrete element method, J. Fluid Mech. 775 (2015) 24–52.
- [20] Y. Guo, C. Wassgren, J.S. Curtis, D. Xu, A bonded sphero-cylinder model for the discrete element simulation of elasto-plastic fibers, Chem. Eng. Sci. 175 (2018) 118–129.
- [21] T. Zhang, M. Zhao, F. Liu, H. Tian, T. Wulan, Y. Yue, D. Li, A discrete element method model of corn stalk and its mechanical characteristic parameters, BioResources 15 (4) (2020) 9337.
- [22] Y. Xia, J. Klinger, T. Bhattacharjee, V. Thompson, The elastoplastic flexural behaviour of corn stalks, Biosyst. Eng. 216 (2022) 218–228.
- [23] T. Leblicq, B. Smeets, H. Ramon, W. Saeys, A discrete element approach for modelling the compression of crop stems, Comput. Electron. Agric. 123 (2016) 80–88
- [24] T. Leblicq, B. Smeets, S. Vanmaercke, H. Ramon, W. Saeys, A discrete element approach for modelling bendable crop stems, Comput. Electron. Agric. 124 (2016) 141–149.
- [25] Y. Xia, Z. Lai, T. Westover, J. Klinger, H. Huang, Q. Chen, Discrete element modeling of deformable pinewood chips in cyclic loading test, Powder Technol. 345 (2019) 1–14.
- [26] Y. Guo, Q. Chen, Y. Xia, J. Klinger, V. Thompson, A nonlinear elasto-plastic bond model for the discrete element modeling of woody biomass particles, Powder Technol. 385 (2021) 557–571.
- [27] Y. Guo, Q. Chen, Y. Xia, T. Westover, S. Eksioglu, M. Roni, Discrete element modeling of switchgrass particles under compression and rotational shear, Biomass Bioenergy 141 (2020) 105649.
- [28] Y. Xia, J. Klinger, T. Bhattacharjee, J. Aston, M. Small, V. Thompson, An experiment-informed discrete element modelling study of knife milling for flexural biomass feedstocks, Biosyst. Eng. 236 (2023) 39–53.

- [29] D. Ramkrishna, A.W. Mahoney, Population balance modeling. Promise for the future, Chem. Eng. Sci. 57 (4) (2002) 595–606.
- [30] D. Ramkrishna, M.R. Singh, Population balance modeling: current status and future prospects, Annu. Rev. Chem. Biomol. Eng. 5 (2014) 123–146.
- [31] L.G. Austin, A preliminary simulation model for fine grinding in high speed hammer mills, Powder Technol. 143 (2004) 240–252.
- [32] R.B. Diemer Jr., Applications of the linear mass-sectional breakage population balance to various milling process configurations, AAPS PharmSciTech 22 (3) (2021) 86.
- [33] L. Vogel, W. Peukert, From single particle impact behaviour to modelling of impact mills, Chem. Eng. Sci. 60 (18) (2005) 5164–5176.
- [34] M. Capece, Population balance modeling applied to the milling of pharmaceutical extrudate for use in scale-up, Adv. Powder Technol. 29 (12) (2018) 3022–3032.
- [35] M. Gil, E. Luciano, I. Arauzo, Approach to the breakage behavior of comminuted poplar and corn stover under single impact, Fuel Process. Technol. 131 (2015) 142–149.
- [36] M. Gil, E. Luciano, I. Arauzo, Population balance model for biomass milling, Powder Technol. 276 (2015) 34–44.
- [37] N. Saha, C. Goates, S. Hernandez, W. Jin, T. Westover, J. Klinger, Characterization of particle size and moisture content effects on mechanical and feeding behavior of milled corn (Zea mays L.) stover. Powder Technol. 405 (2022).
- [38] J.H. Moon, W.B. Yoon, Effect of moisture content and particle size on grinding kinetics and flowability of balloon flower (Platycodon grandiflorum), Food Sci. Biotechnol. 27 (3) (2018) 641–650.
- [39] H. Jung, Y. Lee, W. Yoon, Effect of moisture content on the grinding process and powder properties in food: A review, Processes 6 (6) (2018).
- [40] W. Zhang, Q. Chen, J. Chen, D. Xu, H. Zhan, H. Peng, J. Pan, M. Vlaskin, L. Leng, H. Li, Machine learning for hydrothermal treatment of biomass: A review, Bioresour. Technol. (2022) 128547.
- [41] A. Nag, A. Gerritsen, C. Doeppke, A.E. Harman-Ware, Machine learning-based classification of lignocellulosic biomass from pyrolysis-molecular beam mass spectrometry data, Int. J. Mol. Sci. 22 (8) (2021) 4107.
- [42] H. Cao, Y. Xin, Q. Yuan, Prediction of biochar yield from cattle manure pyrolysis via least squares support vector machine intelligent approach, Bioresour. Technol. 202 (2016) 158–164.
- [43] J.S. Cha, S.H. Park, S.-C. Jung, C. Ryu, J.-K. Jeon, M.-C. Shin, Y.-K. Park, Production and utilization of biochar: A review, J. Ind. Eng. Chem. 40 (2016)
- [44] D.A. Akinpelu, O.A. Adekoya, P.O. Oladoye, C.C. Ogbaga, J.A. Okolie, Machine learning applications in biomass pyrolysis: From biorefinery to end-of-life product management, Digit. Chem. Eng. 8 (2023) 100103.
- [45] C. Lin, Z. Li, L. Lu, S. Cai, M. Maxey, G.E. Karniadakis, Operator learning for predicting multiscale bubble growth dynamics, J. Chem. Phys. 154 (10) (2021) 104118

- [46] L. Lu, X. Meng, Z. Mao, G.E. Karniadakis, DeepXDE: A deep learning library for solving differential equations, SIAM Rev. 63 (1) (2021) 208–228.
- [47] M. Lu, M. Ali, Z. Meng, X. Meng, G. Li, Z. Li, Deep neural operator for learning transient response of interpenetrating phase composites subject to dynamic loading, Comput. Mech. 72 (3) (2023) 563–576.
- [48] N.B. Kovachki, Z. Li, B. Liu, K. Azizzadenesheli, K. Bhattacharya, A.M. Stuart, A. Anandkumar, Neural operator: Learning maps between function spaces with applications to PDEs, J. Mach. Learn. Res. 24 (89) (2023) 1–97.
- [49] L. Lu, P. Jin, G. Pang, Z. Zhang, G.E. Karniadakis, Learning nonlinear operators via DeepONet based on the universal approximation theorem of operators, Nat. Mach. Intell. 3 (3) (2021) 218–229.
- [50] T. Berchem, O. Roiseux, C. Vanderghem, A. Boisdenghien, G. Foucart, A. Richel, Corn stover as feedstock for the production of ethanol: Chemical composition of different anatomical fractions and varieties, Biofuels, Bioprod. Biorefin. 11 (3) (2017) 430–440.
- [51] Jordan Reduction Solutions, JRS G1635 industrial granulator, 2022, https://www.jordanreductionsolutions.com/machine/g1635/index.html [Accessed February 2024].
- [52] L.F.R. Montgomery, G. Bochmann, Pretreatment of Feedstock for Enhanced Biogas Production, IEA Bioenergy Ireland, 2014.
- [53] Y. Xia, T. Bhattacharjee, J. Klinger, E. Fillerup, J. Aston, V. Thompson, Defining particle size distribution of milled biomass: Sieve diameter versus surface area, in: 2023 ASABE Annual International Meeting, American Society of Agricultural and Biological Engineers, 2023, p. 1.
- [54] A. Hamed, Y. Xia, N. Saha, J. Klinger, D.N. Lanning, J. Dooley, Flowability of Crumbler rotary shear size-reduced granular biomass: An experiment-informed modeling study on the angle of repose, Front. Energy Res. 10 (2022) 859248.
- [55] L. Vogel, W. Peukert, Breakage behaviour of different materials—construction of a mastercurve for the breakage probability, Powder Technol. 129 (1–3) (2003) 101–110.
- [56] T. Chen, H. Chen, Universal approximation to nonlinear operators by neural networks with arbitrary activation functions and its application to dynamical systems, IEEE Trans. Neural Netw. 6 (4) (1995) 911–917.
- [57] J.H. Holland, Genetic algorithms, Sci. Am. 267 (1) (1992) 66-73.
- [58] A. Antoniadis, S. Lambert-Lacroix, J.-M. Poggi, Random forests for global sensitivity analysis: A selective review, Reliab. Eng. Syst. Saf. 206 (2021) 107312.
- [59] F. Pedregosa, G. Varoquaux, A. Gramfort, V. Michel, B. Thirion, O. Grisel, M. Blondel, P. Prettenhofer, R. Weiss, V. Dubourg, J. Vanderplas, A. Passos, D. Cournapeau, M. Brucher, M. Perrot, E. Duchesnay, Scikit-learn: Machine learning in python, J. Mach. Learn. Res. 12 (2011) 2825–2830.